Medical University "Prof. dr. Paraskev Stoyanov" – Varna

Faculty of medicine

Department „Anatomy and cell biology"

Martin Nikolaev Ivanov, M.D.

Proliferation and differentiation of progenitor cells in the subventricular zone of the telencephalon of adult monkeys

ABSTRACT of the Dissertation

for the award of the scientific degree of "Doctor"

Scientific Specialty: Anatomy, Histology, and Cytology

Field of Study: 7.1 Medicine

Academic Advisor:

Assoc. Prof. Dr. Stoyan Pavlov Pavlov, M.D., PhD

Varna, 2023

The dissertation is formatted on 147 standard typewritten pages. The literature review is supported by 5 figures. The materials and methods section is supported by 8 figures and 3 tables. The results are supported by 46 figures. The dissertation utilizes 179 literary sources, of which 178 are in English and 1 is in Bulgarian.
The official defense will take place on…..,….., at….., in…… auditorium, combined with a pre-scheduled online meeting.

External Committee members:

1. Prof. Dr. Nikolay Elenkov Lazarov, M.D., Ph.D. - MU-Sofia
2. Assoc. Prof. Dimitrinka Yordanova Atanasova-Dimitrova, Ph.D. - Faculty of Medicine, Trakia University, Stara Zagora
3. Assoc. Prof. Dr. Georgi Nikov Chaldakov, M.D., Ph.D. - MU-Varna

Internal committee members:

1. Prof. Dr. Anton Bozhidarov Tonchev, M.D., Ph.D., D.S.C - MU-Varna
2. Prof. Vanya Goranova Stefovska, M.D., Ph.D. - MU-Varna

Alternate External Committee Member:

Assoc. Prof. Dr. Nikolay Dimitrov Dimitrov, M.D., Ph.D. - Faculty of Medicine, Trakia University, Stara Zagora

Alternate Internal Committee Member:

Assoc. Prof. Dr. Deyan Lyudmilov Dzhenkov, M.D., Ph.D. - Department of General and Clinical Pathology, Forensic Medicine and Deontology, MU-Varna

Table of Contents

1. Summary

Adult neurogenesis is the process of generating new neurons from stem/progenitor cells in the brains of adult individuals. This process occurs in specific regions, referred to as "niches," identified as the subventricular zone of the lateral ventricle and the subgranular zone of the dentate gyrus in the hippocampus (**Fig. 1.1**). The demonstration of proliferating and differentiating cells in these areas in lower mammals (rodents) is well-described and researched. These studies highlight the potential of neural stem cells for the benefits of regenerative medicine. A significant challenge is to find ways to effectively increase the levels of neurogenesis and, consequently, of newly formed neurons capable of integrating into existing neural networks. Substantial differences in cytoarchitecture, cell types, and cell organization in these zones between rodents and humans complicate the reliable translation of the obtained data and their use for clinical research purposes. At the same time, the fate of neural stem cells and their precursors in adult primates, including humans, is debated and poorly studied. Additionally, the presence of reliable markers used to represent cellular subpopulations found in neurogenic zones in rodents, in a large percentage of cases, are not applicable in the study the neurogenesis in primates. This necessitates the use of primate models (non-human-like monkeys) to investigate cellular differentiation, proliferation, and integration because human-like monkeys are phylogenetically closer to humans. The presented study may be of interest both to scientists engaged in fundamental research in the field of neuroscience and life sciences, as well as to specialists involved in translating fundamental research. In this study, we investigate candidate genes that increase after short-term global brain ischemia in the subventricular zone of non-human-like monkeys. The evoked brain ischemia leads to an increase in the proliferation and differentiation of neural stem cells, which is also a good way to screen for candidate genes involved in regenerative and neurogenic processes. Here, we show their topographical localization along the lateral ventricle (rostral-caudal) and demonstrate their phenotype under normal conditions. Due to the possibility of influence through pharmacological treatment, a detailed immunohistochemical phenotyping for APLNR was performed in the normal adult human brain.

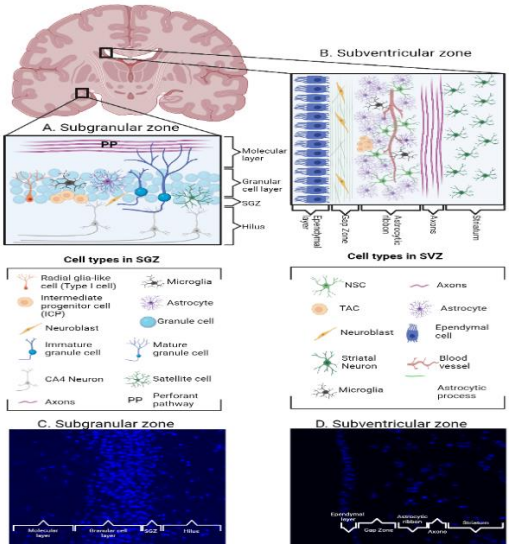

Fig. 1.1: Structure of the Main Neurogenic Niches in Primates: SGZ and SVZ.

A. Structure and cellular composition of the gyrus dentatus, divided into 3 layers: molecular, granular, and subgranular (SGZ). The main cellular subpopulations that are present in those structures are schematically represented, including Type I radial glia, representing the neural stem cells in this zone.

B. Structure and cellular composition of the subventricular zone (SVZ), divided into 4 layers: ependymal layer, gap zone, astrocytic ribbon, and transitional zone, including axons and striatal parenchyma. The main cellular subpopulations that are present in these structures are schematically represented, including B1 astrocytes, representing the neural stem cells in this zone.

C. Micrograph with staining for nuclei (DAPI) of the gyrus dentatus. The three layers of the structure can be distinguished (molecular, granular, subgranular (SGZ)).

D. Micrograph with staining for nuclei (DAPI) of the SVZ. The four layers of the structure can be distinguished: ependymal layer, gap zone, astrocytic ribbon, and transitional zone.

The present dissertation provides a quantitative analysis of the proliferation and differentiation of neural stem cells in adult primates. The results, both from the phenotype of non-human-like primates and humans, may lead to the

discovery of more effective ways to activate neural regeneration and their subsequent use for the treatment of neurodegenerative or psychiatric disorders.

2. Materials and methods

2.1 Selecting the candidate genes for phenotypical analysis

Selection of genes with increased expression in the anterior subventricular zone under normal conditions and after ischemic injury was carried out using the freely available digital database ***monkey-niche.org***, which includes 150 genes functionally related to stem-cell biology. To gain deeper insights into the cellular characteristics of the genes published there, we examined them for interesting expression patterns and localization. Out of the 150 genes, we selected four that showed enhanced expression after ischemic injury, localized and associated with one or more components of the stem-cell zone (blood vessels, expression in the ependymal layer, or strong expression in the subependymal layer). The gene selection was made through visual assessment of gene expression in the area of interest. Gene expression in three regions in controls and after ischemic injury was annotated as follows: Strong expression was marked as "+++", moderate expression as "++", low as "+", and absence of expression as "–". Thus, our selection narrowed down to the genes: APLNR (Apelin Receptor), CD38 (Cluster of Differentiation 38), GJA1 (Gap Junction Alpha-1 protein), and TNC (Tenascin-C). It is important to note that markers like CD133 (Prominin-1), routinely used for the detection of stem cells in the subventricular zone in mice, are not detected in monkeys (PROM1 (CD133) (monkey-niche.org) [1,2]. It is also interesting that CD133 is a factor involved in the Wnt/beta-catenin signaling pathway and protects b-catenin from degradation, and its lack of expression leads to altered proliferation and cell senescence[3].

2.2 Experimental animals and human tissues

For the purposes of our study, seven adult Japanese macaques (Macaca fuscata), belonging to the family Cercopithecidae, Catarrhine

Old World monkeys, were used. These monkeys were divided into: 3 control animals (1 male and 2 females) and 3 ischemic animals (1 male and 2 females), aged between 5-9 years, corresponding to sexually mature young individuals with a weight at the time of the study ranging from 7-10 kg. The monkeys were raised in climate-controlled enclosures with free access to water and food.

All procedures involving experimental animals were carried out with the approval of the respective ethical committees (Japanese monkeys - Ethics Committee of the Institute for Experimental Animals of the Faculty of Medicine, Kanazawa University, Kanazawa, Japan).

For convenience, brain tissues from animals without ischemia will be referred to as "control" in the text, and brain tissues from animals subjected to global ischemia will be referred to as "ischemic".

For optimization of the in situ hybridization protocol, monkey brain tissues were used, provided by the German Primate Center (Deutsches Primatenzentrum), Göttingen, Germany. All animals are offspring of monkeys bred at the center. For convenience in the text, they will be referred to as "calibration".

The human materials used were provided by the Department of General and Clinical Pathology, University Hospital "St. Marina", Varna, with the permission of the Ethics Committee (EC) of Medical University-Varna, protocol No. 86.

All brain materials were collected during routine autopsy, conducted within a post-mortem interval of less than 24 hours, from patients without signs of pathological brain changes and with no history of neuro-psychiatric disorders.

2.3 Surgical procedures

All surgical procedures involving experimental animals were performed by the team of Dr. T. Yamashima at the research unit of the Department of Neurosurgery, Kanazawa, Japan. To induce global ischemia, each monkey was anesthetized (ketamine at a dose of 2-5 mg/kg, i.m.), intubated, and connected to a ventilator. During the surgical procedures, the monkeys were additionally anesthetized by inhalation (1% halothane, gas mixture 40% O2/60% N2O). Arterial blood pressure, pulse, pupil diameter, and reaction were monitored. Throughout the surgery, the body temperature of the animals was maintained at 37±0.5°C.

The surgical procedure associated with global ischemia was performed in sterile surgical conditions in the following sequence: anterior midline thoracotomy, dissection of the skin and subcutaneous tissue, sternotomy, dissection of soft tissues, and visualization of the left subclavian artery and brachiocephalic trunk (***Fig. 2.1***).

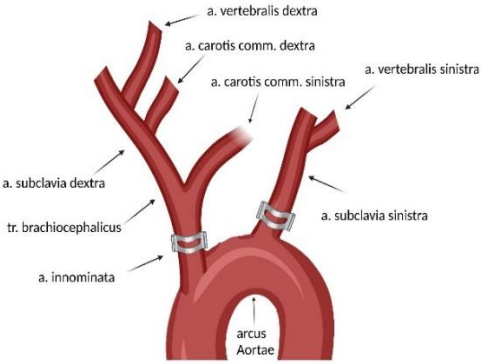

Fig. 2.1: *Experimental Procedure for inducing global ischemia in monkeys: clamps and their position on the arterial blood vessels (left subclavian artery and brachiocephalic trunk/a. innominata) are Shown in Gray. With Modifications* [4]

The latter were clamped with metal clips for 20 minutes at their exit point from the aorta. Subsequently, the clips were removed, blood flow was restored, the chest cavity was closed, and the animals were returned to their cages. Three experimental animals from the control group underwent the same procedures except for the clamping of the left subclavian artery and brachiocephalic trunk.

The animals were euthanized 7 days after the surgical procedure. The brain was extracted from the skull, rapidly frozen in liquid nitrogen, and stored in a freezer maintained at -80°C.

2.4 Tissue processing

The brains were extracted from the cranial vault and immediately frozen in liquid nitrogen. Tissues from the experimental animals were stored at -80°C. For the purposes of FISH (Fluorescence In Situ Hybridization) and IHC (Immunohistochemistry) on some of the tissues containing the aSVZ (anterior Subventricular Zone) and n. caudatus (caudate nucleus), blocks measuring 2 x 2 cm were dissected and subsequently placed at -80°C in O.C.T. (Optimal Cutting Temperature) Compound (Sakura, USA) for one day. The frozen specimens were sectioned using a cryostat microtome (Leica CM3050S) to obtain tissue slices with a thickness of 25 µm, which were then fixed, acetylated, and dehydrated as follows:

Fixation of the specimens with a 4% solution of paraformaldehyde for 25 minutes, followed by rinsing with 0.9% NaCl twice for 2 minutes each. Acetylation was performed using a solution of Tris buffer, acetic acid, and EDTA (TEA buffer). The solution was constantly stirred with a magnetic stirrer. 1 ml of acetanhydride was added to it. The specimens were incubated in the solution twice for 5 minutes with solution replacement. The specimens were then washed in PBS for 2 minutes and in 0.9% NaCl for 2 minutes. Subsequent dehydration was carried out in an ascending series of alcohol: 30%, 50%, 70%, 80%, 95%, and

2x100% (2 minutes for each solution). The specimens were air-dried for 3 minutes at 30°C. Following this procedure, the glass slides with the specimens were sealed in boxes for long-term storage at -80°C [5–8].

2.5 In situ hybridisation staining (colorimetric and fluorescent)

2.5.1 Isolation of RNA

Tissue samples from the subventricular zone (1 cm^3) were dissected from the right hemisphere of at least 3 animals. The dissected blocks were weighed on an electronic balance and divided into batches of 50 mg in microcentrifuge tubes.

Total RNA was isolated using the RNeasy Mini Kit (Qiagen, Germany). For each total RNA isolation, tissue weighing 50 mg was used. Prior to the procedure, the following reagents were added to the kit solutions: 10 µl of beta-mercaptoethanol was added to the RLT buffer (to prevent RNA degradation), and the required amount of 100% ethanol was added to the RPE buffer.

To the microcentrifuge tube containing 50 mg of tissue pieces, 600 µl of RLT buffer was added, and the tissue was homogenized using a tissue homogenizer (Kinematica Polytron PTMR2100). The tissue lysate was centrifuged for 3 minutes at 14,000 rpm, and the supernatant was collected. To the supernatant, 70% ethanol was added, and the solution was transferred to a spin column with a silica membrane, placed in a collection microcentrifuge tube. The column was washed with RW1 buffer and subsequently with RPE buffer. The purified RNA remaining on the silica membrane in the column was eluted with 50 µl of ultrapure water, followed by centrifugation. The quantity and purity of the isolated total RNA were confirmed using a spectrophotometer (NanoDrop 2000/20000c, Thermo Scientific).

2.5.2 cDNA synthesis

Complementary DNA (cDNA) was synthesized from the isolated total RNA using reverse transcriptase (SuperScript III First-Strand Synthesis System for RT-PCR, Thermo Fisher Scientific). Briefly, 2 µg of total RNA was mixed with oligo(dT)20, dNTPs, and DEPC-treated water up to 10 µL. The mixture was incubated at 65°C for 5 minutes. To this solution, appropriate amounts of 10X RT buffer, 5 mM MgCl2, 0.1 M DTT, RNaseOUT™ (40 U/µL), and the reverse transcriptase enzyme SuperScript III RT (200 U/µL) were added. The resulting solution was incubated for 50 minutes at 50°C, followed by heating to 85°C for 5 minutes to terminate the reaction. To degrade the residual RNA in the solution, the necessary amount of RNase H was added, followed by incubation for 20 minutes at 37°C. Unused cDNA was frozen at -80°C [5–8].

2.5.3 Template synthesis

Specific primers (forward and reverse) were designed using the software program Primer3[9]. The constructed primers were 20 nucleotides in length with an approximate CG content of 55% (Table 1). The theoretical length of the amplicon was over 600 kb to better capture the tissue sample. Sequences for T7 and SP6 (T7: GCGTAATACGACTCACTATAGGG, Sp6: GCGATTTAGGTGACACTATAG) necessary for subsequent riboprobe synthesis were added to the constructed primers. To determine the optimal annealing temperature of the primers to cDNA, a temperature-gradient protocol for PCR was used, ranging from 49°C to 62°C. Four aliquots at different temperatures were used, each containing 10x polymerase buffer, 2 mM dNTPs (10mM dNTPs, Roche), Taq polymerase (5 U/µl, Qiagen), 5 µl of cDNA, 10 pmol of forward and reverse primers (100 pmol, MWG Biotech), and Milli-Q water. The PCR machine parameters (Eppendorf 5331 Gradient MasterCycler Thermal Cycler) were as follows: an initial denaturation at 94°C for 2 minutes, followed by 35 amplification cycles of 25 seconds denaturation (94°C), 25 seconds annealing (49° to 62°C), 1 minute and 15 seconds extension (72°C), and a final extension at 72°C for 9 minutes. The resulting

amplicon was analysed on a 1% agarose gel to determine the optimal annealing temperature of the primers to cDNA.

A subsequent second PCR was performed at the established optimal annealing temperature of the primers but in a larger volume. After the procedure, a small portion of the amplicon was analysed on a 1% agarose gel. After purification of the amplicon using a DNA purification kit (PCR Purification Kit, Qiagen, Germany), a small amount of DNA was analysed with a spectrophotometer, and a small portion was sent for sequencing. The process of generating primers, temperature-gradient PCR, final PCR, and purification was repeated for all genes. The products from the final PCR reactions were confirmed by sequencing [5–8].

GENE	ID number (Mucaca Mullata	Forward primer	Reverse primer	Amplicon lenght
GFAP	XM_015119892.1	GCTCCAGGATG AAACCAACC	TAATGACCTCTC CATCCCGC	803
VIM	NM_001284705.1	AATGACCGCTTC GCCAACTA	ACGAAGGTGAC GAGCCATTT	813
APLNR	NM_001047126.1	TGATTTTGACAA CTACTATGGGG CA	ATCGAAGAAGG CATAGAGGAAA GG	925
CD38	NM_001261773.1	GACCCCACCTG GAGCCCTAT	CCATGTATCACC CAGGCCTC	755
TNC	XM_011750403.1	CAGAGGAAGGA GCTCGCTA	GACACCAGGTT CTCCAGCTC	757
GJA1	XM_015137308.1	AGCCTACTCAAC TGCTGGAG	TCGCCAGTAACC AGCTTGTA	831
Prominin-1 (CD133)	EF193352.1	ATGGCCCTTGTA CTTGGCTC	TCCAACGCCTCT TTGGTCTC	812
CALB1	NM_004929.2	GACGGAAGTGG TTACCTGGA	GGTGTACTGAC GGGCCTAAG	924

Table 1: *List of examined genes, their identification number (NCBI), used primers (forward and reverse), and amplicon size.*
N.B. The primers shown do not include added T7 and SP6 sequences..

2.5.4 Riboprobe synthesis

The riboprobes were synthesized through in vitro transcription. A mixture of 1.5 µg of the previously synthesized DNA template along with 2.5 µl of 10x RNA transcription buffer (New England Biolabs), 2.5 µl of 10x DIG (Digoxigenin) or 2.5 µl of 10x Fluorescein labelling mix for RNA marking (Roche), 1.5 µl of Sp6 RNA polymerase (20,000 U/ml, New England Biolabs), 1 µl of RNAase inhibitor (40 U/µl, Thermo Scientific), and DEPC-treated water (Invitrogen) up to a total volume of 30 µl was incubated for 3 hours at 37°C. For double fluorescent in situ hybridization staining, one probe labeled with Digoxigenin (DIG) and one probe labelled with Fluorescein were used. The utilized Digoxigenin or Fluorescein are conjugated with uridine - a glycolyzed pyrimidine analogue attached to ribose. Thus, in the in vitro transcription, each uridine will be bound to Digoxigenin or Fluorescein. This was followed by treatment with 1 µl of DNAse I (Roche), necessary to remove any remaining traces of DNA. For RNA precipitation, 108 µl of 4 M ammonium acetate and 705 µl of 100% ethanol, pre-cooled at -20°C, were added to the obtained solution. The solution was incubated at -80°C for one day. The next day, the samples were centrifuged at 14,000 rpm for 1 hour at 4°C. The resulting supernatant was removed, and the RNA precipitate was washed with 70% ethanol, dried for 2-3 minutes, and eluted in 30 µl of DEPC-treated water (Invitrogen). The obtained riboprobe was quantitatively checked on a spectrophotometer. Hybridization buffer (Ambion) was added to the remaining riboprobe to a final concentration of 100 ng/µl. The samples were stored at -20°C until used for hybridization on the specimens [5–8].

2.5.5 Colorimetric in situ hybridisation staining

To establish the optimal concentration of the riboprobe, colorimetric staining was performed on coronary sections of a calibration monkey brain at the lateral ventricle level. Two concentrations of each riboprobe (500 ng and 1000 ng) were used. The resulting preparations were analysed for the strength of gene expression, and one of the two concentrations was selected for staining the control and ischemic sections of monkey brains.

For chromogenic ISH staining, the following steps were followed:

Rehydration: The sections were pre-thawed from the -80°C freezer and left to equilibrate to room temperature for 20 minutes. The respective sections were rehydrated for 5 minutes with Phosphate-buffered saline (PBS), denatured with 0.2 N HCl for 10 minutes for better probe penetration, and rinsed again with PBS (**Fig. 2.2**). To denature proteins associated with mRNA, the sections were incubated twice with Proteinase K (35-40 µl/100 ml), dissolved in Proteinase K (PK) buffer (1 M Tris-Cl (pH 8.0), 0.5 M EDTA (pH 8.0), and H2O). The sections were washed twice for 5 minutes each with PBS. The sections were fixed with a 4% PFA solution in PBS for 15 minutes and rinsed again twice for 5 minutes in PBS. A pre-hybridization step was performed for 30 minutes at 60°C using hybridization (Hyb) buffer, supplemented with 1 mg/ml dithiothreitol (DTT, Thermo Fisher Scientific). The specific probe concentration, along with tRNA (which aids in riboprobe binding to the respective mRNA), and Hyb buffer were prepared with a volume of 100 µl. The incubation lasted overnight at 60°C. The following day, the sections were washed with sodium citrate solutions of varying concentrations at 60°C to remove unbound probe. This was followed by washing with Phosphate-buffered saline with Tween-20 (PBST) and blocking with 10% inactivated sheep serum, dissolved in PBST. This final step was necessary to prevent non-specific binding of the antibody to antigens due to the subsequent use of a sheep-produced antibody recognizing digoxigenin, incorporated during the in vitro transcription of RNA. The anti-Digoxigenin-AP (Alkaline Phosphatase) antibody was

diluted with 10% inactivated sheep serum in PBST and incubated at room temperature for 1 hour and 30 minutes. The sections were then washed in PBST twice for 20 minutes each. The sections were subsequently treated with TNM buffer supplemented with levamisole, used as an inhibitor of endogenous alkaline phosphatase (5mM Levamisole; pH 9.5). Staining was carried out with a solution of NBT (nitro-blue tetrazolium chloride, Roche) and BCIP (5-bromo-4-chloro-3'-indolyphosphate p-toluidine salt, Roche), dissolved in TNM buffer. The slides were observed under a light microscope for 30 minutes until specific violet staining appeared. The reaction was stopped by rinsing them in PBS three times for 10 minutes each. The slides were covered with Hydro-Mount medium and left to air dry at 37°C for a day [5–8].

All specimens were digitally captured at a resolution of 0.501 µm/pixel using an automated digital slide scanner, the Aperio ScanScope AT2 (Leica Biosystems, Germany).

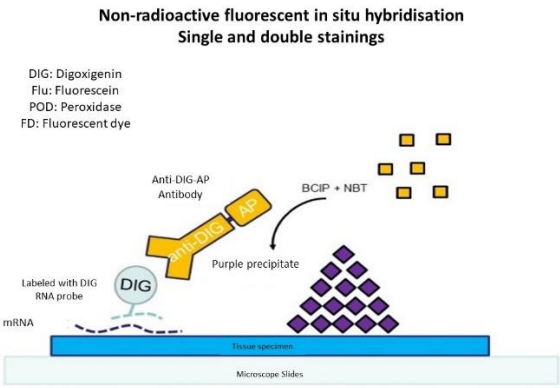

Фиг. 2.2: *Colorimetric in situ hybridization staining depicted schematically. Presented with modifications from 'In Situ Hybridization Methods. Vol. 99' (Springer New York, 2015)* [8].

2.5.6 Rostro-caudal expression of the selected gene in the normal monkey brain

To determine if there was a difference in the rostro-caudal expression of our selected genes, we used three coronary levels corresponding to the most rostral part of the ventricle (+30)[10], the middle part (+23)[10], and the most caudal part (+15)[10] of the ventricle. The coordinates +30, +23, and +15 represent 30 mm, 23 mm, and 15 mm from the intra-auricular line. The selected sections were stained using colorimetric in situ hybridization for the respective genes.

To investigate the precise quantitative increase in these genes after ischemia, we used data from the transcriptomic analysis[5] and software-measured data showing the expression strength of these genes. Quantification was performed by semi-automatic cell counting using the CellDetekt software (version 2.7; https://github.com/tumrod/cellDetekt[11]).

The expression of each of them was measured in the ependymal layer (EL) and subependymal layer (SEL) along the entire length of the ventricle, as well as in a randomly selected region in the striatum (200 x 200 μm) using the CellDetekt software[11]. The software identifies the location of the cells and the degree of expression of the given gene, categorizing them into the following categories: (1.) in red: cells with very strong expression of the gene; (2.) in blue: cells with strong expression; (3.) in yellow: cells with weak expression; (4.) in gray: cells without expression; (5.) in black: background without cells. The ratio of category (1.) and (2.) to all cells in both conditions was calculated, as well as the corresponding fold increase in gene expression in control compared to ischemia[5].

Additionally, statistics were performed on the relative expression of the specified genes, determined from the transcriptomic analysis (RNA-seq, RNA sequencing), reported as the number of gene copies normalized to the total number of gene copies from three control and three ischemic monkeys [5].

2.5.6 Rostro-caudal proliferation in the normal monkey brain

To quantify the proliferating cells along the rostro-caudal axis of the ventricle, we utilized immunohistochemical staining for the proliferative marker Ki67. In brief, the specimens underwent antigen retrieval (DAKO PT Link, Germany) in citrate buffer (pH 6) at 97°C for 5 minutes, followed by cooling on ice for 30 minutes. The specimens were rinsed with PBS three times for 5 minutes and blocked for 1 hour with 10% (Cat. No S-1000, Vectorlabs) normal goat serum, dissolved in PBS with 0.1% Tween-20. Primary antibodies were incubated in combination with the blocking solution overnight at 4°C. The next day, the slides were rinsed in PBS three times for 5 minutes and incubated for 2 hours at room temperature with secondary antibodies, conjugated with AlexaFluor-555 (Thermo Fisher Scientific, Germany). Subsequently, the slides were rinsed with PBS three times for 5 minutes and covered with a mounting medium (ProLong Gold Antifade Mountant, Thermo Fisher Scientific, USA) [5]. The specimens were imaged using an epifluorescent microscope Zeiss AxioImager Z.2 (Carl Zeiss GmbH), equipped with a fully motorized stage and monochrome CCD camera AxioCam Mrm rev.3 (Carl Zeiss GmbH). Due to the small number of positive cells (<50), the cells were manually counted on each slide throughout the dorsal-ventral extent of the ventricle. For visualization clarity, each positive cell was marked as a red dot on the corresponding image at the respective level. The images used were taken from "A Combined MRI And Histology Atlas Of The Rhesus Monkey Brain In Stereotaxic Coordinates" [10].

2.5.8 "Rostral-caudal analysis of gene expression in different mammals using open databases

To conduct the rostro-caudal analysis, open-access databases containing information on the gene expression of TNC, APLNR, CD38, and GJA1 in three coronal levels corresponding to the most rostral (+30)[10], middle (+23)[10], and most caudal (+15)[10] parts of the ventricle in Mus musculus, Callithrix jacchus, and Macaca fuscata were used.

Various anatomical markers (e.g., the location of the third ventricle opening) were utilized for orientation. The gene expression was semi-quantified by counting positive cells using the CellDetekt software along the entire length of the ventricle in all three species. The expression of each gene was measured in the subependymal layer (SEL) along the entire length of the ventricle and in a randomly selected region in the striatum (200 x 200 µm) using the CellDetekt software. Different settings were applied for processing in the three animal species (***Fig. 2.3***). The software itself identifies the cell localization and determines the degree of gene expression, categorizing them as follows: (1.) red: cells with very strong expression of the gene; (2.) blue: cells with strong expression; (3.) yellow: cells with weak expression; (4.) gray: cells without expression; (5.) black: background without cells.

The data for Callithrix jacchus were obtained from the ISH atlas at the Institute of Physical and Chemical Research (Riken), Japan (Marmoset Gene Atlas (*brainminds.jp*)). The data for Mus musculus were obtained from the ISH atlas at the Allen Institute for Brain Science, USA (file download date: 20.03.2022). The specimens from Macaca fuscata were prepared by us through manual colorimetric in situ hybridization (See 5.5.5. Colorimetric in situ hybridization).

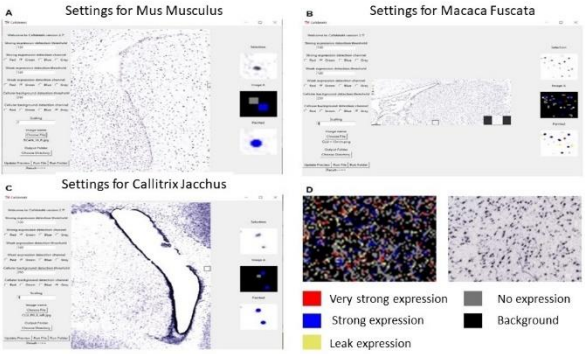

Fig. 2.3: *Settings used in CellDetekt for Mus musculus (A), Callithrix jacchus*

(C), and Macaca fuscata (B). An example image showing the result obtained after using CellDetekt, with color-coded categorization of the expression level (D).

2.5.9 Fluorescent in situ hibridisation staining

For fluorescent in situ hybridization (FISH) staining, the following protocol was used:

All solutions were prepared with DEPC-treated water, and all steps were carried out at room temperature, unless otherwise stated below. The specimens were pre-extracted from the -80°C freezer and allowed to equilibrate to room temperature for 20 minutes (***Fig. 2.4***). Endogenous peroxidase was blocked with 3% H2O2 in methanol, prepared immediately before incubation. The sections were rinsed twice for 5 minutes each with Phosphate-buffered saline (PBS). They were then denatured with 0.2 N HCl for 10 minutes to enhance probe penetration and rinsed again with PBS. To denature mRNA-associated proteins, the sections were incubated twice with Proteinase K (35-40 µl/100 ml) dissolved in activating PK buffer (1 M Tris-Cl (pH 8.0), 0.5 M EDTA (pH 8.0), and H2O). The sections were washed twice for 5 minutes each with PBS. The sections were fixed with 4% PFA in PBS for 15 minutes and again rinsed twice for 5 minutes with PBS. Pre-hybridization was performed for 30 minutes at 60°C with Hyb buffer supplemented with 1 mg/ml dithiothreitol (DTT, Thermo Fisher Scientific). The specific probe concentration, labeled with digoxigenin (for single FISH), was prepared in a solution containing tRNA (to facilitate binding of the riboprobe to the corresponding mRNA) and Hyb buffer (total volume of 100 µl). Incubation continued for one day at 60°C. In cases of double FISH labeling, one of the probes was labeled with digoxigenin, and the other with fluorescein, both at the appropriate working concentrations.

The next day, the specimens were rinsed with sodium citrate solutions of varying concentrations at 60°C to wash away unbound RNA probe. This was followed by a wash with Phosphate-buffered saline with 0.1%

Tween-20 (PBST) and blocking with 10% inactivated sheep serum, dissolved in TNB (Tris-HCl (pH 7.5), NaCl, and 0.5% blocking reagent (PerkinElmer, FP1020)). The latter step was necessary to prevent non-specific binding of antibodies due to the use of sheep-derived antibody in the next step, which recognizes digoxigenin incorporated during in vitro transcription of RNA. The anti-digoxigenin (peroxidase) antibody was diluted with 10% inactivated sheep serum in TNB and incubated at room temperature for 30 minutes. In cases of double FISH labeling, the anti-fluorescein (peroxidase) antibody was also used.

The specimens were rinsed with TNT (Tris-NaCl-Tween buffer) three times for 5 minutes each. Fluorescent labeling was achieved with a working solution of tyramide containing the appropriate fluorophore-labeled tyramide (Cy3), diluted in 1x amplification buffer. Incubation with the latter solution lasted for 3 minutes. The aim of these final steps was to convert the inactive tyramide into an active form through the action of peroxidase on the antibody, leading to its deposition around the RNA of interest [12,13]. The specimens were rinsed three times for 5 minutes each in TNT to terminate the reaction.

For dual FISH staining, the specimens were rinsed in 0.2 M HCl for 15 minutes and three times for 15 minutes each in TNT buffer. Treatment with HCl aimed to remove anti-digoxigenin peroxidase. They were blocked with sheep serum in TNB for 15 minutes. The anti-fluorescein peroxidase antibody was applied for 30 minutes, followed immediately by a 15-minute wash with TNT buffer. For visualization of the reaction, a working solution of tyramide containing fluorescein-labeled tyramide (FITC) was used for 7-10 minutes. The reaction was stopped by rinsing with TNT buffer for 15 minutes [12,13]. All fluorescent specimens were counterstained with the nuclear marker DAPI for 5 minutes.

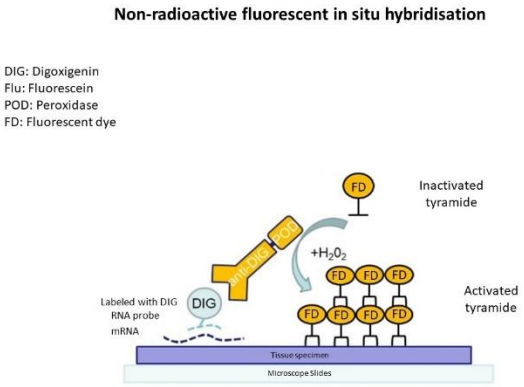

Fig. 2.4: *Schematic representation of fluorescent in situ hybridization (FISH) staining. Presented with modifications from "In Situ Hybridization Methods. Vol. 99" (Springer New York, 2015)*[8].

Single or double FISH stainings were additionally combined with various antibodies, as presented in Table 2.

Following single or double FISH staining, the samples underwent antigen retrieval (DAKO PT Link, Germany) in citrate buffer (pH 6) at 97°C for 5 minutes, followed by cooling on ice for 30 minutes. The samples were rinsed with PBS three times for 5 minutes each and blocked for 1 hour with 10% normal goat serum (Cat. No S-1000, Vectorlabs) dissolved in PBS with 0.1% Tween-20. Primary antibodies were incubated in combination with blocking solution overnight at 4°C. The next day, the slides were rinsed in PBS three times for 5 minutes each and incubated for 2 hours at room temperature with secondary antibodies conjugated with AlexaFluor-488 or AlexaFluor-647 (Thermo Fisher Scientific, Germany). The slides were then rinsed with PBS three times for 5 minutes each and covered with a mounting medium (ProLong Gold Antifade Mountant, Thermo Fisher Scientific, USA)[5].

Antibody	Species	Dilution	Company and cat. No
anti-BrdU	rat	1:100	Cat. No Ab6326, Abcam, Cambridge, United Kingdom
anti -GFAP	mouse	1:400	Cat. No M0761, Dako-Agilent Technologies GmbH, Hamburg, Germany
anti -GFAP	chiken	1:1000	Cat. No AB5541, Merck Millipore
anti -GLUT1/SLC2A1	rabbit	1:100	Cat. No HPA031345, Sigma-Aldrich
anti -Vimentin	mouse	1:1000	Cat. No MAB3400, Merck Millipore
anti -Apelin receptor (APLNR)	mouse	1:100	Cat. No MAB856, R&D Systems
anti -DCX	goat	1:50	Cat. No sc-8066, Santa Cruz
anti -S100b	rabbit	1:200	Cat. No Z0311, DAKO
anti -GFAP-delta	rabbit	1:1000	Cat. No AB9598, Sigma-Aldrich
anti -Ki67	rat	1:50	Clone TEC-3, DAKO

Table 2: *List of used antibodies, their type, and application for the purposes of this study.*

Antibody	Manufacturer	Cat. No.	Dilution
Rb 488	Thermo Fisher Scientific	A11008	1:300
Rb 555	Thermo Fisher Scientific	A27039	1:300
Rb 647	Thermo Fisher Scientific	A27040	1:300
Mo 647	Thermo Fisher Scientific	A-21235	1:300
Gt 488	Thermo Fisher Scientific	A-11078	1:300
Gt 596	Thermo Fisher Scientific	A-11055	1:300
Chk 555	Thermo Fisher Scientific	A-21437	1:300

Rat 594	Thermo Fisher Scientific	A-11007	1:300
Gt 555	Thermo Fisher Scientific	A-21432	1:300

Table 3: *Lists of secondary antibodies used in the study, Used abbreviations: Rb, rabbit; Mo, mouse; Gt, goat; Gpig, guinea pig; Chk, chicken.*

2.6 Protocol for the BrdU staining

5-bromo-2'-deoxyuridine (BrdU, Sigma Chemicals, St. Louis, MO, USA) was dissolved in 0.9% NaCl. One experimental animal was injected with a dose of 100 mg/kg i.v. for 5 days (total amount of BrdU for the monkey is 500 mg/kg). The monkey was euthanized 2 hours after the last BrdU injection. BrdU can also be incorporated into apoptotic cells, but previous studies conducted on the same monkeys have shown that staining is specific only for proliferating cells and does not accumulate in apoptotic ones [14,15]. Based on these data, no staining for apoptosis markers was performed in this study.

2.7 Phenotypic Analysis of APLNR in the Normal Human Brain

For the purpose of phenotyping APLNR+ cells in the normal brain (without any signs of pathological or neuro-psychiatric changes), three human brains were used. These brains were dissected by the same researchers, and the same anatomical landmarks were always for orientation. All dissected brains were obtained from routine autopsies with a post-mortem interval of <24h. The dissected tissues included the anterior part of the lateral ventricle along with the underlying part of the n. caudatus. After the dissection, the tissues were briefly rinsed in PBS, then fixed in fresh 4% PFA solution for 24 hours at 4°C. This was followed by a 24-hour wash in running water and subsequent cryoprotection with increasing concentrations of sucrose solution (10, 15, 30% solution). Subsequently, they were placed at -80°C in O.C.T. (Tissue-Tek O.C.T. (Optimal Cutting Temperature) Compound, Sakura, USA) for one day. The frozen specimens were sectioned on a cryostat microtome (Leica CM3050S) into tissue slices with a thickness of 25

µm. The specimens were left to dry at 37°C for one day. The next day, the specimens were subjected to antigen retrieval (DAKO PT Link, Germany) in citrate buffer (pH 6) at 97°C for 5 minutes, followed by cooling on ice for 30 minutes. The specimens were rinsed with PBS three times for 5 minutes each and blocked for 1 hour with 10% (Cat. No S-1000, Vectorlabs) normal goat serum, dissolved in PBS with 0.1% Tween-20. The primary antibodies (Table 2) were incubated in combination with blocking solution for one night at 4°C. The next day, the slides were rinsed in PBS three times for 5 minutes each and incubated for 2 hours at room temperature with secondary antibodies (Table 3), conjugated with AlexaFluor-488, 555, or 647 (Thermo Fisher Scientific, Germany). Then, the slides were rinsed with PBS three times for 5 minutes each and covered with a mounting medium (ProLong Gold Antifade Mountant, Thermo Fisher Scientific, USA) [5]. The specimens were imaged using an epifluorescent microscope Zeiss AxioImager Z.2 (Carl Zeiss GmbH), equipped with a fully motorized stage and monochrome CCD camera AxioCam Mrm rev.3 (Carl Zeiss GmbH). The counting of double-positive cells was performed manually on coronal sections along the length of the ventricle (dorso-ventrally).

2.8 Control experiments and staining

1. The specificity of ISH and immunohistochemical staining was confirmed through negative and positive control stainings.
2. When performing the Polymerase Chain Reaction (PCR), we used a positive control for CALB1 with the exclusion of Taq polymerase. In these amplifications, no DNA bands were observed when analyzing the gel electrophoresis results.

Negative Control Stainings:

1. ISH, FISH: Negative controls for ISH and FISH were stained with all steps except for the incubation with the RNA riboprobe itself. In all specimens treated in the absence of the RNA riboprobe, no staining was observed (***Fig. 2.5***).

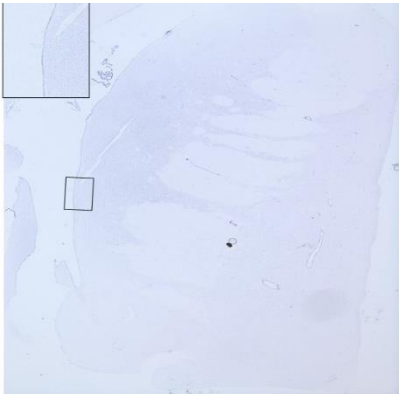

Fig. 2.5: *A specimen incubated in the absence of the riboprobe shows no staining (negative control).*

2. Antibodies: When staining with antibodies, the sections were processed through all steps except for the primary antibody incubation. All specimens treated without primary antibodies remained immunonegative.

1. BrdU: In order to exclude false-positive staining for BrdU, parallel stainings were performed on tissues from monkeys not treated with BrdU, in addition to the tissues from BrdU-injected monkeys. Furthermore, negative controls were conducted where no anti-BrdU antibody was incubated. In both described cases, no BrdU staining was observed.
2. PCR: For polymerase chain reaction, we used a negative control that included all components except for Taq polymerase. In these amplifications, no DNA bands were observed upon analysis of the gel electrophoresis results.

Positive controls:

1. To confirm the specific staining of BrdU, tissues with proliferating cells (intestinal epithelium) from monkeys treated with BrdU were used. These clearly exhibited nuclear staining.

2. To test the specificity of the antibodies used, immunohistochemical stainings were performed on sections taken from organs where there is data on the expression of the respective protein (e.g., APLNR - liver; ***Fig. 2.6***).

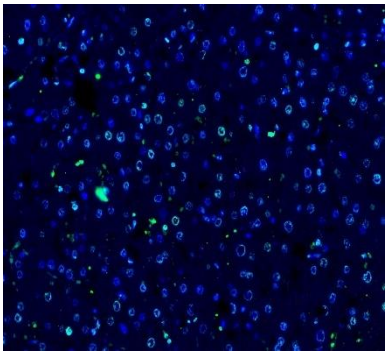

Fig. 2.6: *The specimen incubated with the APLNR antibody displays specific staining for the protein in the hepatic tissue.*

As a positive control staining for ISH and FISH, the CALB1 (Calbindin 1) probe at a concentration of 100 ng/ml was used due to its abundant expression in the CNS (***Fig. 2.7***).

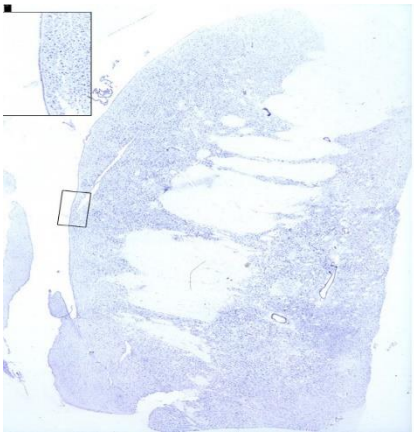

***Fig. 2.7**: The specimen incubated with the CALB1 riboprobe shows specific staining for this gene and was used as a positive control.*

2.9 Image aquisition

The samples were observed and captured using Axio Vision 4.9 software (Carl Zeiss GmbH) on an epifluorescent microscope Zeiss AxioImager Z.2 (Carl Zeiss GmbH), equipped with a fully motorized stage and monochrome CCD camera AxioCam Mrm rev.3 (Carl Zeiss GmbH). For our experiments, the samples were imaged in two ways:

1. High-quality overview image (captured in mosaic mode) of the periventricular tissue, taken with an EC Plan-Neofluar 20x/0.50 objective with a lateral resolution of 0.65 μm/px.

2. 3 to 5 images of fields from the SVZ on a glass slide with the z-stack function, taken with an EC Plan-Neofluar 40x/0.75 objective with a lateral resolution of 0.325 μm/px and an axial resolution (z-distance) between 0.125 and 0.55 μm. The z-stacks were captured as a sequence starting from the most dorsolateral edge of the ventricle, moving towards the medial plane. The acquired images were further processed.

The camera was set with a 2x2 binning factor to reduce the scanning time of the samples and the background noise of the camera. Shading

from uneven illumination was corrected during the capturing process using the built-in shading correction of the camera, using pre-recorded images of the illumination field from fluorescent test slides. All camera settings for the different channels were kept constant. When necessary, exposure was variable to avoid saturation, which is more detrimental to image analysis than differences in exposure time. The images were saved in the native unprocessed format (.zvi) of the Axio Vision software, and after stitching individual images from the captured sample, they were exported in 16-bit TIFF format for further processing and analysis.

2.10 Image processing

Our main goal was to reduce operator-dependent systematic deviation and develop an automated algorithm for processing and analyzing images with a standardized, reproducible approach to a set of images with variable distribution of signal and/or background brightness.

The processing and analysis of the images were performed using the FIJI/ImageJ software[16,17] and partly in CellProfiler[18,19]. All images were processed using the same algorithm.

1. 2-D Projection of Z-stack: The 20 µm thick slices contain spatial 3-D information. We decided to capture a Z-stack of the regions of interest and create a 2-D projection of the focused pixels. For this purpose, we used the Smooth Manifold Extraction [20,21] (SME) projection algorithm with the SME projection plugin in FIJI/ImageJ (https://github.com/biocompibens/SME/). The algorithm effectively extracts only the focused sections of the Z-stack and removes out-of-focus light, which can complicate image segmentation and processing.

2. Denoising: The resulting projection images were processed to remove excess noise using the "Non-Local Means" algorithm with automatic standard deviation (sigma) calculation for noises[22], again using FIJI/ImageJ software (https://imagej.net/Non_Local_Means_Denoise).

3. Top-Hat Filtering: Top-Hat filtering was performed using the MorphoLibJ[23] library available in FIJI/ImageJ (https://imagej.net/MorphoLibJ). Top-Hat filtering is a type of morphological filter. A structural element with known size and dimensions is compared to the elements present in the image, and it is filtered based on its relationship to this structural element [24]. This type of morphological filtering relies on morphological "opening," which is subtracted from the original image. The morphological "opening" itself is a sequence of "erosion" (removing pixels from the image that correspond to the structural element), followed by "dilation" (adding pixels to an object that the structural element does not fit). This procedure removes objects smaller than the structural element, while preserving the size of the remaining elements. The reverse procedure is called "closing," where dilation is followed by erosion, leading to the removal of "holes" (dark areas) smaller than the structural element. Since "opening" removes any object smaller than the size of the structural element, the result is equivalent to the background, which does not contain our "interesting" objects. Therefore, "Top-Hat" (top minus hat) is a procedure for subtracting the background, preserving only objects of the same or smaller size than the one used in the opening.

To minimize possible artifacts, we performed the "Top-Hat" filter with the following modifications:

a. Instead of using "classic" opening and closing (as described above), we performed opening through reconstruction. This way, the erosion of the image is reconstructed through geodesic dilation until it "fits" into the original image (instead of using the structural element) [24].

b. Before "opening through reconstruction," the background "holes," which may create false peaks after subtraction, were removed

through "closing through reconstruction" - dilation followed by geodesic erosion."

The investigated markers and their channels on the different slides were grouped based on the expected similarity in the local spatial distribution of the image signal into three groups - (i) DAPI and BrdU; (ii) FISH images; and (iii) extranuclear FIHC (fluorescent immunohistochemistry in combination with FISH) images. The images in each group were measured using granulometry, and the upper confidence limit (p=0.05) of the mean geometric size of characteristic objects for the group was chosen as the radius (r) of the structural element (maximum size of retained particles) for Top-Hat filtering. Thus, DAPI, BrdU, and FIHC of nuclear antigens were processed with R=13px, while FISH and extranuclear FIHC images with R=11px. The steps of the "Top-Hat" procedure were as follows:

1. Morphological dilation of the original image with a disc-shaped structuring element with a radius of r.

2. Morphological reconstruction through erosion of the expanded image from the original image (start = expanded image, mask = original image, connectivity = 8).

3. Morphological erosion of the closed image with a disc-shaped structuring element with a radius of r.

4. Morphological reconstruction through expansion of the "eroded" image from the "closed" image (start = expanded image, mask = closed image, connectivity = 8), which is an approximation of the background without objects smaller than r.

5. Arithmetic subtraction of the background from the original image. Z-score normalization of image intensity:

The filtered images were converted to 32-bit format, and the pixel intensity was scaled to Z-scores:

$Z_{pixel} = \frac{Pixel\ Intensity\ - Mean\ Intensity}{Standard\ Deviation\ of\ Intensity}$ (Mean intensity = 0 и Standard Deviation = 1).

This way, the value of each pixel is equal to the number of standard deviations its intensity is from the mean intensity of the image (for example, a pixel value of -1 means that the intensity of this pixel is one standard deviation lower than the mean intensity of the image before transformation).

1. Generation of regions of interest (RoIs)

DAPI channels were further segmented using CellProfiler software with an algorithm based on intensity and shape. The program settings were the only step where processing parameters were selected by a human operator. Cellular RoIs were generated by expanding the nuclear RoIs by 2 μm, controlling for overlap: for boundaries between overlapping RoIs, we used Voronoi transformation boundaries of segmented nuclei. Staining with BrdU reduces the quality of staining, and consequently, of DAPI. Therefore, we processed the BrdU channel (where present) with the same settings as the DAPI images and added those RoIs that do not overlap with the ones generated from DAPI RoIs. This way, we eliminated possible deviation introduced by weaker/missing DAPI staining (especially in BrdU-positive nuclei). As a final step for analysis, only those regions of interest that were detected within 150 μm from the base of the ependymal layer were selected.

2. Z-score Thresholding

The majority of each fluorescent image is occupied by background. This fact can be interpreted that the signal occupies positive distant pixels (with grayscale value greater than a few standard deviations in the positive direction from the mean value of the image). A significant portion of any remaining background from the measurement (i.e., non-DAPI) channels was excluded from the analysis by setting 0 for all pixels with a Z-score result smaller than 1 (more likely to belong to the background).

2.11 Image analysis

1. Classification of RoI

The classification of RoIs was performed semi-automatically with a customized counting script in FIJI/ImageJ software. The script sequentially performs the following actions: (i) loads the RoI set and the processed channels of the image to be measured, (ii) isolates the signal using an iterative Li thresholding algorithm to minimize cross-entropy for each channel, (iii) measures the positive area within each 'cellular' RoI in all loaded channels, (iv) assigns a label based on the 'positivity' of the RoI in each channel, (v) draws an annotated image of RoIs, and (vi) records the number of RoIs belonging to each class. Depending on the different combinations of marker expression (positive or negative), different RoIs are labeled as belonging to one of 8 (when three channels are measured) or 4 (for two-channel assessments) classes.

2.12 Data analysis and statistics

We performed an analysis of the ROC curve[25] to choose suitable overlap thresholds for the classification algorithm. This was done for several metrics (mean gray value, unprocessed integrated density, proportion of signal area after the automatic Li thresholding algorithm, which calculates a global threshold for separating signal from background) using ~300 randomly selected RoIs in SEL, which were evaluated by an experienced researcher as positive or negative for each marker in the respective images. The ROC curves showed good agreement between the three metrics and expert classification, and the fraction of above-threshold area by Li was chosen as the easiest to implement in the counting automation script. The images were divided into three groups depending on the primary type of marker detection and the expected similarities in their local spatial distribution - FISH, nuclear markers, and extra-nuclear IHC markers. Thresholds were calculated for each group separately: for FISH images and extra-nuclear FIHC images, thresholds were chosen (see image analysis) that maximize the sum of sensitivity (true positive rate) and specificity (true negative rate), while for nuclear markers, due to the small relative number of positive cells, we preferred to maximize specificity.

From the counting data, we generated absolute and relative frequency tables for each valid combination of investigated markers (i.e., markers co-stained and assessed together in one or more slides). Due to the non-homogeneous nature of the data, we chose to generate confidence intervals for the fractions of cellular classes using non-parametric Monte Carlo pseudo-sampling[26,27]. We developed a scheme for random sampling of cells, simulating the way cells are actually counted: each set of classified RoIs for a valid combination of markers (stained and assessed together in the same images) was examined through 100,000 random sub-samples of random sizes, ranging from 25% to 75% of the number of RoIs in the set. Each sub-sample was generated by random sampling with replacement from the overall set of valid RoIs. This approach with variable-sized cell sub-samples mimics the way cells are counted on images with different sizes of sampling areas (different-sized parts of SVZ are chosen for cell counting). Assuming that all cells checked for a specific combination of markers are representative of the entire cell population (e.g., cells in adult SEL of control primates), then the sub-sample simulates the counting of a multitude (e.g., 100,000 images). This approach is based solely on the measured data and can provide a good estimate of the error in our measurements. It should be interpreted only from this perspective (not as representative of the entire animal population). The differences between the observed and each of the repeatedly taken mean fractions of the respective cell classes were calculated, and the quantiles 0.025 and 0.975 were used as estimates of the lower and upper bounds of the 95% confidence interval (i.e., the interval at p=0.05) for each cellular fraction[27]. Data processing (e.g., generating frequency tables) and analysis were performed using the R language and environment for statistical computing v.3.4.4 [28] in RStudio IDE[29] and additional libraries tidyverse, pROC, vcd, vcdExtra, and epitools [30,31].

---

* Random sampling with replacement is performed, where after each selected member of the respective sample, it is returned to the overall set for subsequent random selection. This way, the set of elements for selection becomes infinitely large

3.Results

3.1 Analysis of Gene Expression Characteristics in the Public Database monkey-niche.org

To better understand the expression profile of various genes with increased expression in the anterior subventricular zone under normal conditions and after ischemic injury, we utilized the publicly available digital database *monkey-niche.org.* This information system encompasses 150 genes functionally linked to stem cell biology[5]. All genes were visually inspected for expression levels in four regions of interest and annotated based on their expression level.

3.2 Analysis of the expression characteristics of TNC (Tenascin-C)

When visually assessing the images from Monkey-Niche displaying TNC expression, we observed the following: in the control monkey, individual cells with moderate mRNA expression in the SVZ were observed (+). Additionally, there was moderate to strong expression in the EL (+). In contrast to the healthy control, in the ischemic animal, cells were clustered with strong expression (+++). Furthermore, an increased presence of positive cells around blood vessels was observed (PVSVZ+), which was absent in the control (-). Expression in the ependymal layer was enhanced (+++) compared to the control stainings (***Fig. 3.1***).

Quantitative assessment with CellDetekt showed that TNC-expressing cells in the EL increased on average by 1.2-fold (EL - fold change - 1.2, 95% confidence interval 46.52% - 59.02%) after global ischemia compared to control animals (EL - 1, 95% confidence interval 20.20% - 32.08%), while TNC-expressing cells in the SVZ increased on average by 1.7-fold (SVZ - 1.7, 95% confidence interval 29.18% - 34.58%) compared to control animals (SVZ - 1, 95% confidence interval 15.78% - 20.98%) (***Fig. 3.1 E***). The same results were observed when comparing transcriptomic data (***Fig. 3.1 F***). Dorso-ventral expression gradient were not found in both control and ischemic stainings.

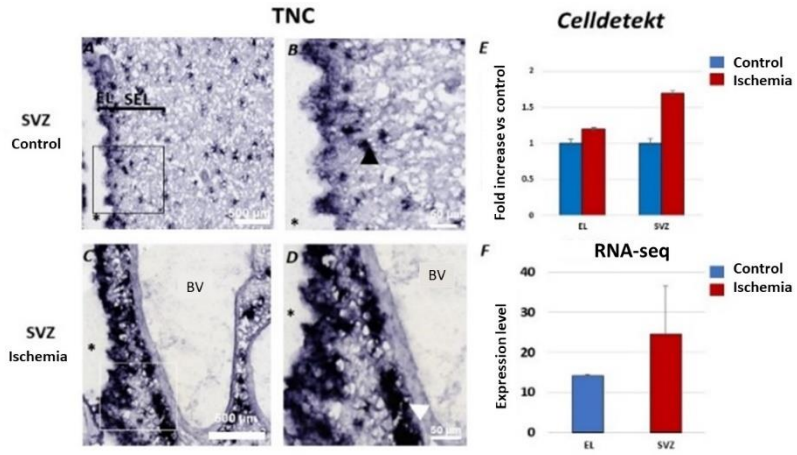

***Fig. 3.1**: (**A-B**) TNC mRNA staining in normal conditions:*

(A). (A) presents the SVZ, containing EL and SEL in the control. Moderate ISH expression is observed in both EL and SVZ. (B). Zoom-in of the highlighted area in A. Individual cells are observed in SEL (black arrow) and moderate expression along the entire length of the ependyma.

(C-D). TNC mRNA staining after ischemia: (C). (C) shows the SVZ, containing EL, SVZ, and a blood vessel (BV) after ischemia. Strong expression is observed in both EL and SVZ with cell conglomerates (white arrow in D.) and enhanced presence around the BV. (D). Zoom-in of C, showing numerous cells in close proximity to the blood vessel (white arrow) and directly under the ependymal layer.

(E). Data from CellDetekt measurements. Fold change in RNA expression in EL and SVZ after ischemia.

(F). Data from transcriptomic analysis (RNA-seq) [5]. Relative expression of TNC, expressed as the number of gene copies in control and after ischemia. The lateral ventricle is marked with an asterisk. BV - blood vessel..

3.3 Analysis of the expression characteristics of APLNR (Apelin receptor)

On the specimens uploaded to monkey-niche.org and stained for APLNR mRNA, we observed individual cells with weak expression in the SVZ (+) (***Fig. 3.2***). Weak expression is also detected in the EL (+). After ischemia, the cells are clustered just below the EL and exhibit strong expression (+++). The expression in the ependymal layer is significantly amplified compared to the control stains. Perivascular staining is not observed in control stains (-), but it is present in ischemic animals (+).

Quantitative assessment with CellDetekt reveals that APLNR-expressing cells in EL increase on average by 2-fold (EL - fold change - 2.065, 95% confidence interval 46.75% - 59.95%) after global ischemia compared to control animals (EL - 1, 95% confidence interval 20.29% - 31.21%), while those in SVZ increase by an average of 2.4 times (SVZ - fold change - 2.411, 95% confidence interval 10.36% - 15.36%) compared to control animals (SVZ - 1, 95% confidence interval 3.52% - 7.05%) (***Fig. 3.2 E***). Transcriptomic data show an approximately 18-fold increase in transcripts compared to the control. Neither in the control nor in the ischemic staining was there evidence of a dorso-ventral expression gradient (***Fig. 3.2 F***).

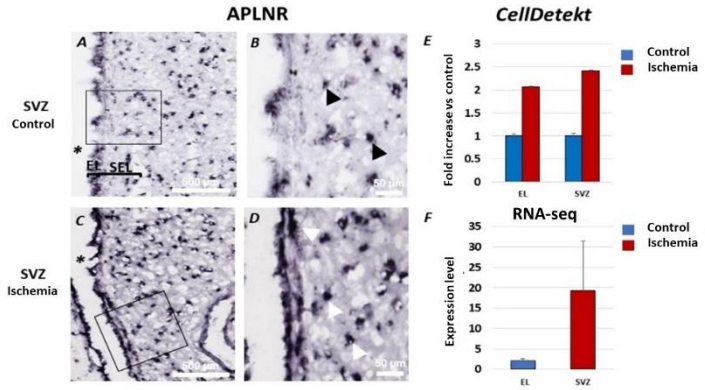

Fig. 3.2*: (A-B) Staining for APLNR mRNA in normal conditions: (A) In (A), SVZ containing EL and SVZ is observed. Our observations show weak ISH expression*

both in EL and SVZ. (B) Magnification of the marked area in A. Individual cells in SEL are observed (black arrow) along with low expression along the entire length of the ependyma.

(C-D) Staining for APLNR mRNA after ischemia: (C) In (C), SVZ containing EL, SEL after ischemia is observed. Very strong expression is noted both in EL and SVZ with clusters of cells present (white arrow in D). (D) Magnification of C, showing numerous cells in immediate proximity and directly below the ependymal layer.

(E) Data from measurement with CellDetekt. A manifold increase in mRNA expression in EL and SVZ after ischemia.

(F) Data from transcriptomic analysis[5]*. Relative expression of APLNR, expressed as the number of gene copies in control and after ischemia. The lateral ventricle is marked with *.*

3.4 Analysis of the expression characteristics of GJA1 (Gap Junction Alpha-1 protein)

In the preparations stained for GJA1 mRNA, we observed individual cells with weak to moderate expression in the SVZ (++). Weak expression was also observed in the EL (+). In ischemic animals, clusters of cells with strong expression formed immediately below the EL (+++). Increased expression was also noted around blood vessels (PVSEL+), with no staining observed in the vascular wall itself. The SVZ also exhibited enhanced staining for GJA1 mRNA compared to the controls (+++).

Quantitative assessment using CellDetekt and transcriptomic data confirmed the upregulation of GJA1 gene expression following ischemia (***Fig. 3.3 E and F***). Our measurements revealed that GJA1+ cells in the EL increased by 1.2 times following ischemia (EL - fold change - 1.240, 95% confidence interval 42.24% - 55.35%) compared to non-ischemic animals (EL - 1, 95% confidence interval 33.28% - 45.40%). In the SVZ, a 1.5-fold increase was observed (SVZ - 1.576, 95% confidence interval 19.24% - 24.58%) compared

to the same region in control animals (SVZ - 1, 95% confidence interval 11.48% - 16.24%). No dorso-ventral gradient was observed in either staining.

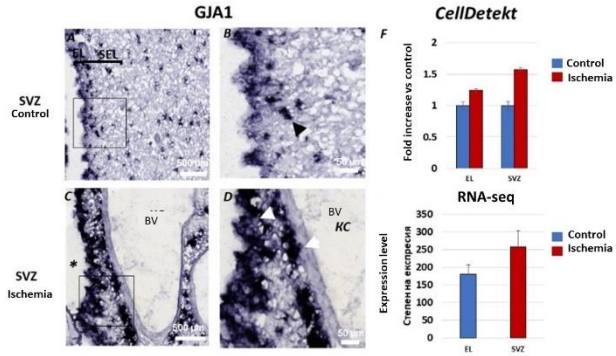

***Fig. 3.3**: (**A-B**) Staining for GJA1 mRNA in normal condition: (A) In (A), the SVZ containing EL and SEL in a control animal is observed. Moderate ISH expression is observed in both EL and aSVZ. (B) Enlargement of the marked area from A. Individual cells are observed in SEL (black arrow), with moderate presence of mRNA along the entire length of the ependyma.*

(C-D) Staining for GJA1 mRNA after ischemia: (C) In (C), the SVZ containing EL, SEL, and a blood vessel (BV), after ischemia is observed. Very strong expression is observed in both EL and SVZ, with massive accumulations of cells (white arrow in D) around the BV. (D) Enlargement of C, showing numerous cells in immediate proximity to the blood vessel (white arrow) and directly beneath the ependymal layer.

(E) Data from measurement with CellDetekt. Fold increase in mRNA expression in EL and SVZ after ischemia.

*(F) Data from transcriptomic analysis (RNA-seq) [5]. Relative expression of GJA1, expressed as the number of gene copies in control and after ischemia. * denotes the lateral ventricle.*

3.5 Analysis of the expression characteristics of CD38 (Cluster of differentiation 38)

For specimens stained for CD38 mRNA, we observed individual cells with weak to moderate expression in the SVZ (+). Additionally, there was no expression detected in the EL (-). In ischemic animals, clusters of cells with strong expression formed immediately beneath the EL (+++). Increased expression was also noted around blood vessels (PVSEL +), although no staining was present in the vessel walls. The SVZ exhibited enhanced staining for CD38 mRNA compared to controls (+++).

Quantitative analysis with CellDetekt and transcriptomic data confirmed the upregulation of CD38 gene expression following ischemia (***Fig. 3.4 E and F***). Measurements revealed that CD38+ cells in the EL did not show an increase after ischemia compared to animals without ischemia. In the SVZ, a 30-fold increase was observed (SVZ - 30, 95% confidence interval 28.09% - 33.45%) compared to the same region in control animals (SVZ - 1, 95% confidence interval 13.33% - 15.33%). No dorso-ventral gradient was observed in either staining.

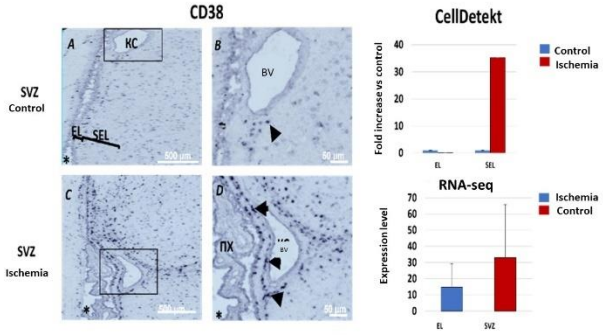

***Fig.3.4**: (**A-B**) Staining for GJA1 mRNA in normal conditions: (A) In (A), the SVZ containing EL and SEL in a control animal is observed. Moderate ISH expression is noted in both EL and aSVZ. (B) Zoomed-in view of the marked area in A. Individual cells are visible in SEL (black arrow) with moderate mRNA presence along the entire length of the ependyma.*

Staining for GJA1 mRNA after ischemia: (C) In (C), the SVZ containing EL, SEL, and a blood vessel (BV) during ischemia is shown. Strong expression is observed in both EL and SVZ with massive cell clusters (white arrow in D) around the BV. (D) Zoomed-in view of C, showing numerous cells in immediate proximity to the blood vessel (white arrow) and directly beneath the ependymal layer.

(E) Data from measurement with CellDetekt. Marked increase in mRNA expression in both EL and SVZ after ischemia.

*(F) Data from transcriptomic analysis (RNA-seq) [5]. Relative expression of GJA1, quantified as the number of gene copies in control and after ischemia. Lateral ventricle is indicated by *.*

3.6 Phenotypic analysis of the selected genes

Adult neuronal stem/progenitor cells are multipotent and capable of self-renewal, proliferation, and differentiation into neurons and glia[32]. The stem/progenitor cells express proteins such as GFAP, Vimentin, GLAST, CD133, Nestin, ASCL1 (Mash1), EGFR, BrdU, and others[33]. It is important to note that there is no single marker for identifying the different heterogeneous subpopulations of stem/progenitor cells (qNSCs, aNSCs, TAPs, neuroblasts). For this reason, the combination of the mentioned markers and the genes we investigated can provide a clearer understanding of the nature of each subpopulation.

For this purpose, we used the following fluorescent immunohistochemical or FISH staining in combination with FISH for the respective genes of interest:

1. GFAP (Glial fibrillary acidic protein) was used as a marker for qNSCs, aNSCs, and parenchymal astrocytes.
2. Vimentin was used as a marker for aNSCs, TAPs, and endothelium.
3. BrdU (5-bromo-2'-deoxyuridine) was used as a marker for dividing cells. Due to the nature of BrdU application in the experimental animals, BrdU will be primarily incorporated into rapidly dividing cells of the TAPs type and some dividing aNSCs.

4. To characterize the APLNR+ population, GLUT1 (Glucose transporter 1) was used to label blood vessels.

3.7 Phenotypic analysis of TNC (Tenascin-C)

Immunohistochemical staining for GFAP, Vimentin, and BrdU was performed in combination with FISH for TNC. The staining revealed the presence of TNC+/GFAP+ cells (22.9% of all cells in aSVZ), TNC+/Vimentin+ cells (27.3%), and TNC+/BrdU+ cells (1.4%).

To investigate whether there are proliferating GFAP+/TNC+ cells, we conducted double immunohistochemical staining for GFAP and BrdU in combination with FISH for TNC. The results indicate that only 1.3% of all DAPI+ cells are triple-positive cells (TNC+/GFAP+/BrdU+) (***Fig. 3.5 A-E***).

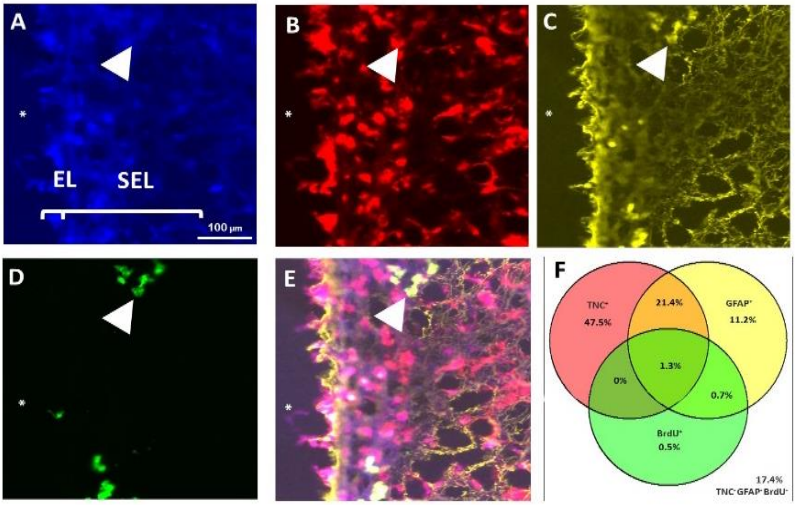

Fig. 3.5*: (**A-E**) Staining for TNC mRNA (B) (red) in combination with GFAP (C) (yellow) and BrdU (D) (green). All nuclei are stained with DAPI (A) (blue). The triple-positive cell (TNC+/GFAP+/BrdU+) is indicated by the arrowhead.*

(F) Venn diagram depicting the different cellular subpopulations: BrdU+, TNC+, GFAP+, BrdU+/TNC+, GFAP+/TNC+, GFAP+/BrdU+, TNC+/GFAP+/BrdU+, and TNC-/GFAP-/BrdU-. Percentages represent the proportion of each fraction of all DAPI+

cells. The ventricular lumen is marked with an asterisk.

3. Phenotypic analysis of APLNR

Fluorescent immunohistochemical staining was performed for GFAP, Vimentin, BrdU, and Glut1 in various combinations with FISH for APLNR. Our stainings revealed the presence of APLNR+/GFAP+ (50.5% of all cells), APLNR+/Vimentin+ (26.5%), APLNR+/BrdU+ (1.9%), and APLNR+/Glut1+ (12.2%) cells.

In the triple staining for APLNR, GFAP, and VIM, we found that triple-positive cells APLNR+/GFAP+/VIM+ accounted for 9.9% of all DAPI+ cells (***Fig. 3.6 A-E***).

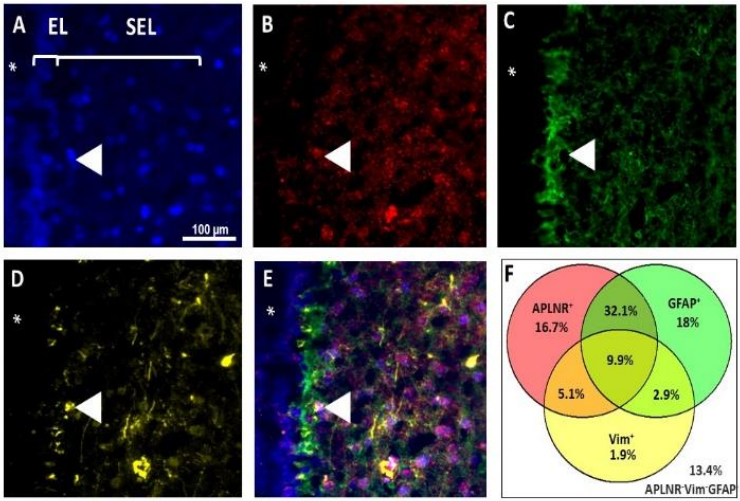

***Fig. 3.6**: **(A-E)** Staining for APLNR mRNA (B) (red) in combination with GFAP (C) (green) and Vimentin (D) (yellow). All nuclei are stained with DAPI (A) (blue). An arrowhead indicates a triple-positive cell APLNR+/GFAP+/Vim+.*

(E) Percentage of the individual cellular subpopulations: APLNR+, Vim+, GFAP+, APLNR+/Vim+, APLNR+/Vim+/GFAP+, and APLNR-/GFAP-/Vim- out of all cells. The

ventricular lumen is marked with an asterisk.

3.9 Phenotypic analysis of GJA1 (Gap Junction Alpha-1 protein)

Similarly, a phenotypic analysis of GJA1 was conducted using the aforementioned markers. Fluorescent immunohistochemical staining for GFAP, Vimentin, and BrdU in combination with FISH for GJA1 was performed. The staining revealed the presence of GJA1+/GFAP+, GJA1+/Vimentin+, and GJA1+/BrdU+ cells. The percentage of double-positive cells was 21.8%, 7%, and 2% respectively.

In a triple combination for BrdU, GFAP, and GJA1, our results showed that 0.6% of all cells were triple-positive for GJA1, GFAP, and BrdU. Single-positive cells for GJA1 were 15.2%, for BrdU and GFAP, 0.2% and 27.9% respectively (***Fig. 3.7 A-E***).

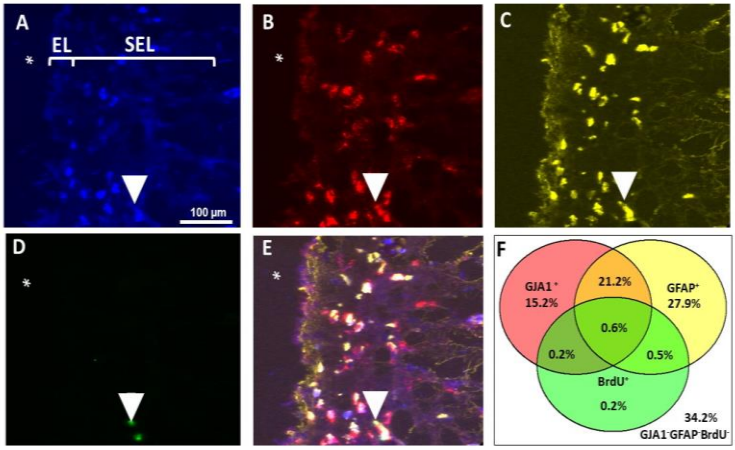

Fig. 3.7*: (**A-E**) Staining for GJA1 mRNA (B) (red) in combination with GFAP (C) (yellow) and BrdU (D) (green) was performed. All nuclei were counterstained with DAPI (A) (blue). Triple-positive cells for GJA1+/BrdU+/GFAP+ are indicated with arrowheads.*

(F) Venn diagram illustrating the different cellular subpopulations: GJA1+, BrdU+, GJA1+/GFAP+, GFAP+/GJA1+, GJA1+/BrdU+, and GJA1-/BrdU-/GFAP-. The percentages represent the respective fraction of all DAPI+ cells. The ventricular lumen is marked with an asterisk..

3.10 Phenotypic analysis of на CD38

Fluorescent immunohistochemical staining for GFAP, Vimentin, and BrdU in combination with FISH for CD38 was performed. Our stainings revealed the presence of CD38+/GFAP+, CD38+/Vimentin+, and CD38+/BrdU+ cells. The percentage of double-positive cells was 31.9%, 11.9%, and 1.3% respectively.

In a triple combination for VIM, GFAP, and CD38, our results show that 8.4% of all cells are triple-positive for the indicated markers (***Fig.3.8 A-E***). Single-positive cells for CD38 are 15.4%, for VIM - 3%, and for GFAP - 21.2%.

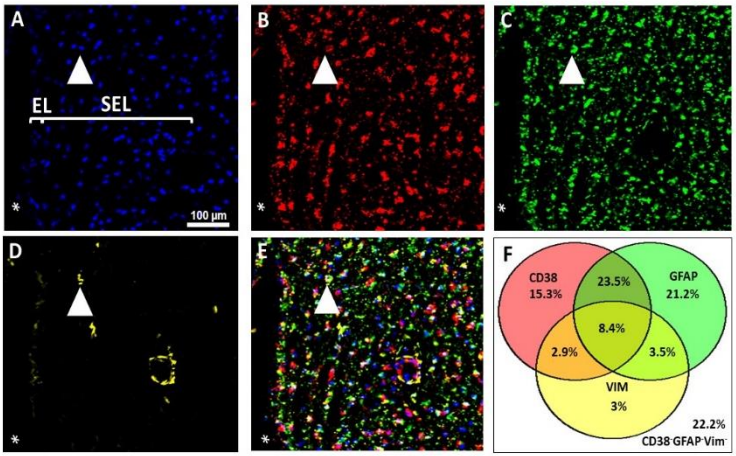

***Fig. 3.8**: (**A-E**) Staining for CD38 mRNA (B) (red) in combination with GFAP (D) (green) and VIM (E) (yellow) was performed. All nuclei are stained with DAPI (A) (blue). A triple-positive cell CD38+/GFAP+/VIM+ is marked with an arrowhead.*

(F) Venn diagram representing the different cellular subpopulations: GFAP+, CD38+, VIM+, GFAP+/CD38+, VIM+/CD38+, GFAP+/VIM+/CD38+, GFAP+/VIM+, GFAP-/VIM-/CD38-. The percentages reflect the proportion of each fraction out of all DAPI+ cells..

3.11 Co-expression between some of the selected genes

Since TNC and GJA1 represent a subpopulation of qNSCs or aNSCs, we used double FISH staining for both genes and found that 36.5% of all cells are double-positive for both genes, while 33.4% and 2.9% are single-positive for TNC and GJA1, respectively (***Figure 3.9***). To investigate the phenotype of the identified subpopulation of cells, we performed double FISH in combination with immunohistochemical staining for BrdU and Vimentin.

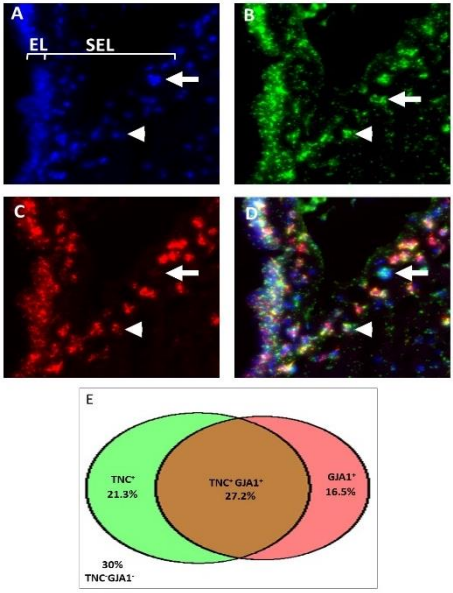

***Fig. 3.9**: (**A-D**) Staining for TNC mRNA (B) (green) in combination with GJA1 (C) (red). All nuclei are stained with DAPI (A) (blue). An arrowhead indicates a TNC+ cell that is negative for GJA1. An arrow indicates a double-positive cell for GJA1+/TNC+. (E) Venn diagram depicting the different cellular subpopulations: TNC+, GJA1+, TNC+/GJA1+, and TNC-/GJA1-. Percentages represent the respective fraction of all DAPI+ cells.*

After counting, we found that the triple-positive subpopulation of TNC+/VIM+/GJA1+ cells accounts for 7.2%, while the proportion of double-positive TNC+/VIM+ cells is 7.9% (***Fig. 3.10***). Interestingly, we observed the presence of a subpopulation of TNC-/GJA1+/VIM+ cells, and the TNC-/GJA1+ subpopulation does not express Vimentin.

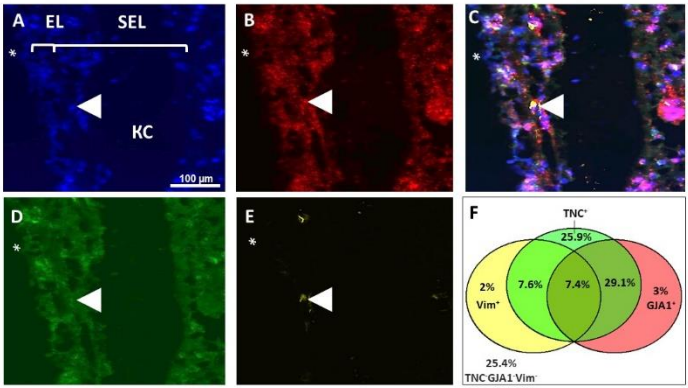

***Fig. 3.10**: (**A-E**) Staining for TNC mRNA (D) (green) in combination with GJA1 (B) (red) and Vimentin (E) (yellow). All nuclei are stained with DAPI (A) (blue). A triple-positive cell GJA1+/TNC+/VIM+ is marked with an arrow. (E) Shows a compilation of (A), (B), (C), and (D). A single positive cell GJA1+/TNC-/VIM- is marked with an arrowhead.*

(F) Venn diagram depicting the different cellular subpopulations: TNC+, GJA1+, TNC+GJA1+ and TNC-/GJA1-/VIM-, VIM+/TNC+ and VIM+/GJA1+. Percentages reflect the proportion of each fraction of all DAPI+ cells.

Additionally, we performed fluorescent immunohistochemical staining for the combination of TNC and GJA1 with BrdU (***Fig. 3.11***). From the obtained results, we found that the TNC-/GJA1+ subpopulation not only does not express Vimentin, but also does not include cells that have incorporated BrdU into their nucleus.

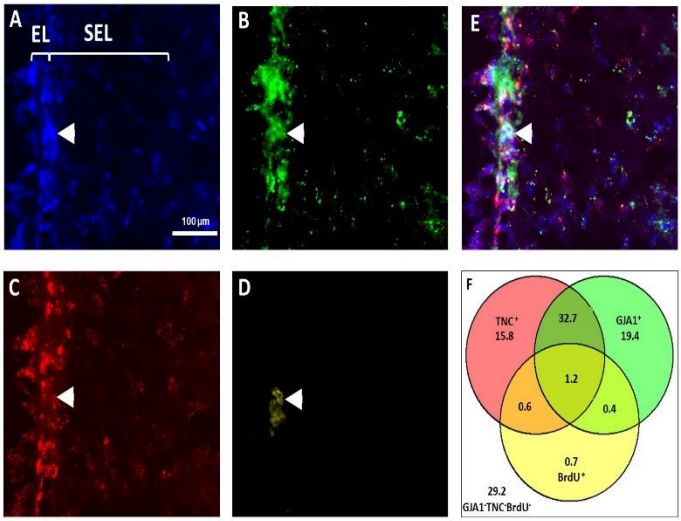

***Fig. 3.11**: (**A-E**) Fluorescent immunohistochemical staining for GJA1 mRNA (B) (green) in combination with TNC (C) (red) and BrdU (D) (yellow). All nuclei are stained with DAPI (A) (blue). A group of double-positive cells for GJA1+/BrdU+ is indicated by the arrowhead, which are negative for TNC. (F) Percentage ratio of the individual cellular subpopulations: TNC+, GJA1+, TNC+/GJA1+, and TNC-/GJA1-BrdU-, BrdU+/TNC+, and BrdU+/GJA1+ of all cells.*

3.11 Phenotype of APLNR positive cells in the SVZ of a control human brain

The high expression of APLNR in the monkey brain, the presence of literature data on the involvement of the apelinergic system in normal physiological and pathophysiological processes, and the fact that APLNR can be used as a pharmacological target motivated us to further investigate the expression of APLNR in the subventricular zone of the normal human brain. To understand whether APLNR is expressed in this zone, we used immunohistochemical methods to stain human brain samples with a post-

mortem interval of <24 hours (***Fig. 3.12***). Our results demonstrated the presence of the protein in the area of interest. The human subventricular zone is composed of three layers: ependyma, gap zone, and subependymal layer containing an astrocytic ribbon. Expression of APLNR is observed in all three layers of the zone.

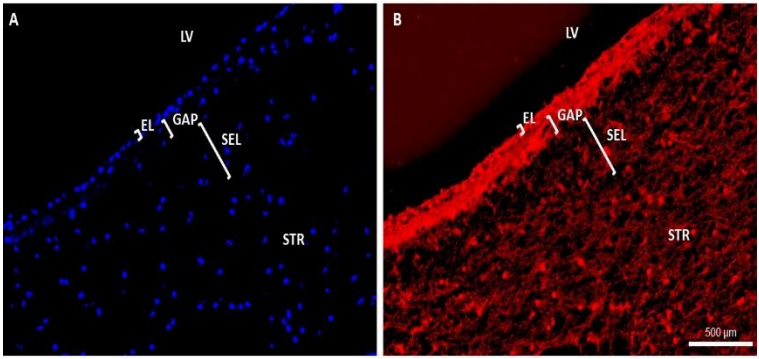

***Fig. 3.12**: (**A-B**) Immunohistochemical staining for APLNR (B) (red). All nuclei are stained with DAPI (A) (blue). APLNR is strongly expressed in the of interest.*

Our statistical analysis reveals that in the hypocellular zone, APLNR-positive cells account for 56% (95% confidence interval 55.63% - 57.12%) compared to the astrocytic ribbon, where they make up about 47% (95% confidence interval 46.95% - 47.88%) of all DAPI-marked cells (***Fig. 3.13***).

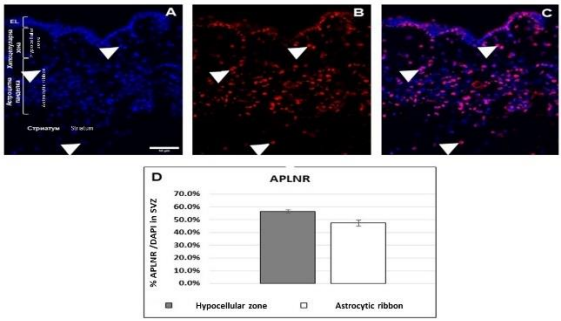

***Fig. 3.13**: (**A-C**) Immunohistochemical staining for APLNR (B) (red). All nuclei are stained with DAPI (A) (blue). (D) Percentage of APLNR content in the hypocellular zone and astrocytic ribbon of the SVZ.*

To understand which cellular subpopulations in the human subventricular zone (SVZ) express APLNR, we performed double immunohistochemical staining for GFAP, GFAP-delta, DCX, and Ki67.

Results from double fluorescent immunohistochemical staining with APLNR and GFAP revealed that APLNR is expressed in GFAP+ cells and their processes in the astrocytic ribbon. We found that APLNR is expressed in GFAP+ cells in the SVZ. Dual staining with APLNR and GFAP, a marker for both NSCs and astrocytes, showed that of all APLNR+ cells in the astrocytic ribbon, approximately 55% of them are GFAP+ (95% confidence interval 43.68% - 55.03%).

Comparing this percentage between the three dorso-ventral regions, we observed that in the ventral SVZ, the ratio of double-positive cells to the total number of APLNR-expressing cells is significantly increased. It's important to note that GFAP is not a specific marker for NSCs, as it can also be expressed by parenchymal astrocytes.

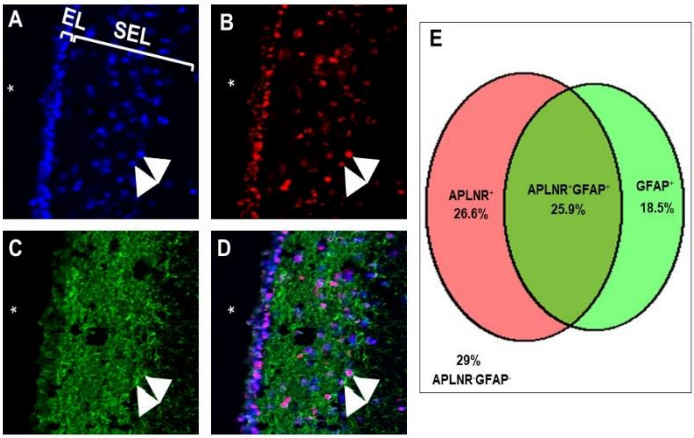

***Fig. 3.14**: (**A-C**) Immunohistochemical staining for APLNR (A) (red) and GFAP (B) (green) is shown. All nuclei are stained with DAPI (blue). Double-positive cells for APLNR and GFAP are observed, indicated by the arrowhead in the subependymal layer (SEL). (D) Percentage distribution of the individual cellular subpopulations: APLNR+, GFAP+, APLNR+/GFAP+, and APLNR-/GFAP- out of all cells.*

Ki67 (Proliferating Cell Nuclear Antigen) is a proliferative marker that labels dividing cells. To determine the quantity of dividing cells in the SVZ of humans and whether the APLNR+ subpopulation proliferates, we used triple fluorescent immunohistochemical staining with antibodies against APLNR, GFAP, and Ki67 in the normal human brain. We observed that Ki67+ cells along the entire length of the ventricle were few (17 cells out of a total of n=3 counted coronal sections) (***Fig. 3.15***). Of these 17 cells, 14 were positive for APLNR, accounting for 82% of all Ki67+ cells. Two were positive for both APLNR and GFAP, and one was negative for both APLNR and GFAP (***Fig. 3.15***). All of them were located in layer II (gap zone) or layer III (astrocytic ribbon).

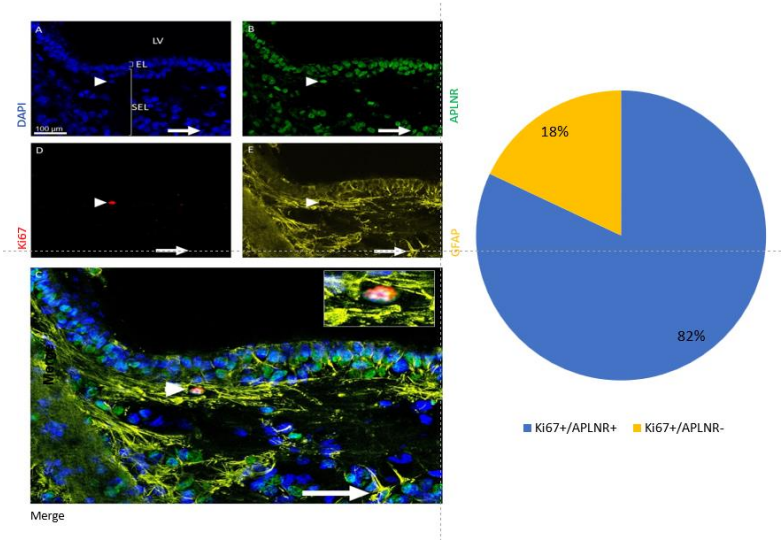

***Fig. 3.15**: (A-E) Immunohistochemical staining for APLNR (B) (green), Ki67 (D) (red), and GFAP (E) (yellow). All nuclei are stained with DAPI (A) (blue). An individual double-positive cell for APLNR and Ki67 is marked with an arrowhead. A double-positive cell*

for APLNR and GFAP is marked with an arrow. The micrograph in the upper left corner of (C) shows an enlargement of a Ki67+ cell.

To determine whether APLNR is expressed in bona fide NSCs in the human subventricular zone, we performed dual immunohistochemical staining for GFAP-delta and APLNR. We found that APLNR is expressed in GFAP-delta+ cells and their processes in the astrocytic ribbon.

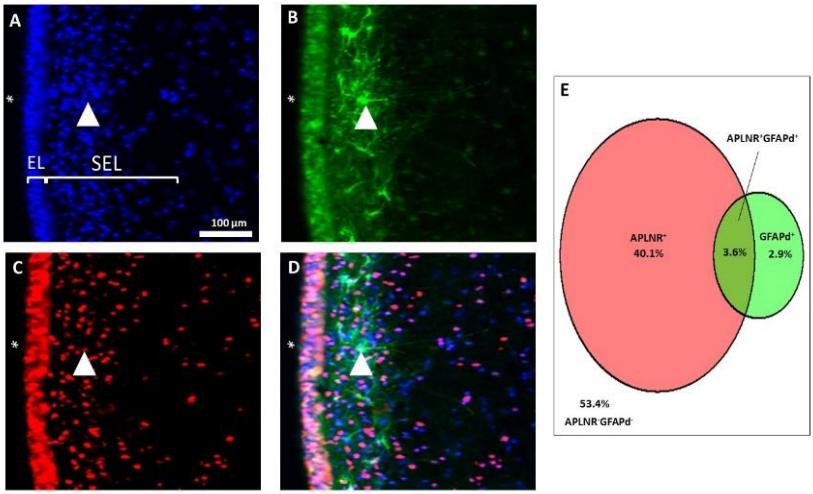

***Fig. 3.16**: (**A-D**) Immunohistochemical staining for APLNR (in red) and GFAP-delta (in green) is shown. All nuclei are stained with DAPI (in blue). Cells that are double-positive for both APLNR and GFAP-delta are indicated with arrows. The percentage distribution of the individual cellular subpopulations—APLNR+, GFAPd+, APLNR+/GFAPd+, and APLNR-/GFAPd-—is presented relative to all cells.*

The co-staining for APLNR and GFAP-delta, an isoform of GFAP found exclusively in qNSCs, reveals that double-positive cells are approximately 8% (95% confidence interval 6.75% - 9.63%). In the dorso-ventral axis, there is a significant increase in this ratio in the mid-ventricular regions.

To distinguish between neural stem/progenitor cells and post-mitotic parenchymal astrocytes, we used the calcium-binding protein S100B (***Figure***

3.17). Our results show that in the hypocellular zone, 11% (95% confidence interval 9.58% - 12.02%) of all APLNR+ cells are double-positive, representing displaced ependymal cells compared to the astrocytic ribbon, where almost 25% of them are jointly marked for this marker, corresponding to mature astrocytes (95% confidence interval 18.41% - 25.98%).

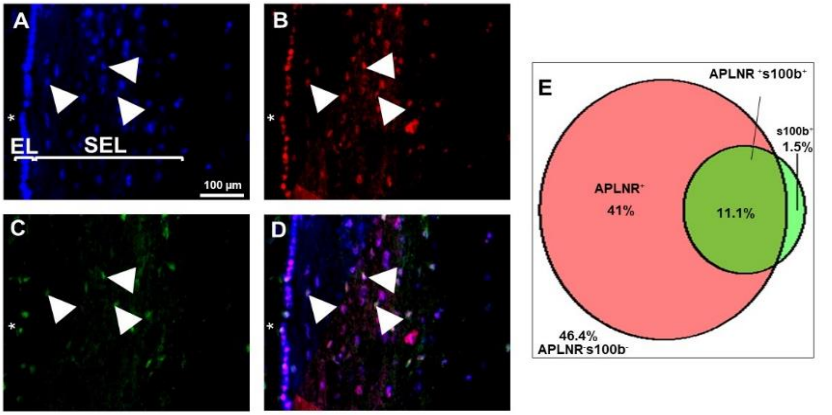

***Fig. 3.17**: (**A-E**) Immunohistochemical staining for APLNR (B) (red) and s100b (C) (green). All nuclei are stained with DAPI (A) (blue). Double-positive cells for APLNR and s100b are indicated by arrowheads. Percentage distribution of individual cell subpopulations: APLNR+, s100b+, APLNR+/s100b+ and APLNR-/s100b- among all cells.*

During their developmental stage, neural stem/progenitor cells begin to differentiate, initially transforming into amplifying cells - a type of rapidly dividing cells. These amplifying cells, in turn, differentiate into immature neurons or neuroblasts. Neuroblasts migrate along the RMS to the OB, where they differentiate into interneurons. Neuroblasts can be identified using antibodies targeting DCX (doublecortin) and β-III-tubulin. Cellular functions such as motility, migration, and mitosis are associated with the proper binding and stabilization of microtubules[34,35]. These processes are regulated by microtubule-associated proteins like DCX. During neurogenesis, DCX and

β-III-tubulin play roles in the proliferation and migration of neuroblasts towards the OB.

Double stainings were performed with β-III-tubulin (***Fig. 3.18***). The statistics show a decrease in the proportion of double-positive cells out of all APLNR+ cells from dorsal to ventral in the hypocellular zone.

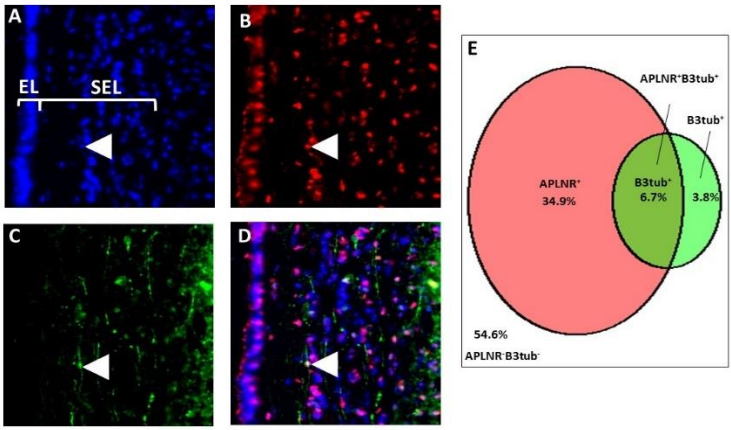

Fig. 3.18 *(**A-D**) Fluorescent immunohistochemical staining for APLNR (B) (red) and β-III-tubulin (C) (green) was performed. All nuclei are stained with DAPI (A) (blue). A double-positive cell for APLNR and β-III-tubulin in SEL is marked with an arrowhead (D). The percentage of individual cell subpopulations is shown: APLNR+, b3tubb+, APLNR+/b3tubb+, and APLNR-/b3tubb- out of all cells (E).*

Fluorescent double immunohistochemical staining for Iba1 and APLNR (***Fig. 3.19***) was performed to understand if microglial cells, the primary phagocytic cells in the brain, express APLNR. Our results show that out of all APLNR+ cells, 41% of them in the hypocellular zone are double-positive for Iba1 (95% confidence interval 40.35% - 42.54%), compared to the astrocytic ribbon, where they are 12% (95% confidence interval 11.41% - 13.76%).

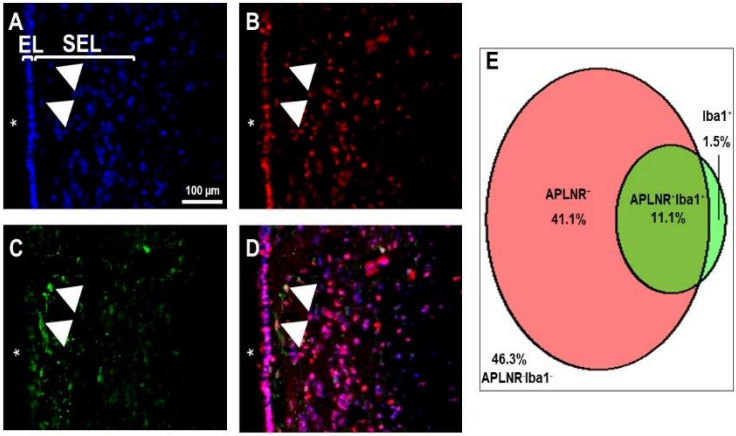

***Fig. 3.19**: (**A-D**) Immunohistochemical staining for APLNR (B) (red) and Iba1(C) (green) was performed. All nuclei are stained with DAPI (A) (blue). A double-positive cell for APLNR and Iba1 is marked with an arrowhead in SEL (D). The percentage ratio of individual cellular subpopulations - APLNR+, Iba1+, APLNR+/Iba1+, and APLNR-/Iba1- - is shown for all cells (E).*

To determine whether the brain endothelial cells express APLNR, we performed double fluorescent immunohistochemical staining for GLUT1 and APLNR (***Fig. 3.20***). Our results showed that nearly 5% of all APLNR+ cells are endothelial cells positive for GLUT1, both in the perivascular space and in the astrocytic endfeet (95% confidence interval 2.96% - 6.51%).

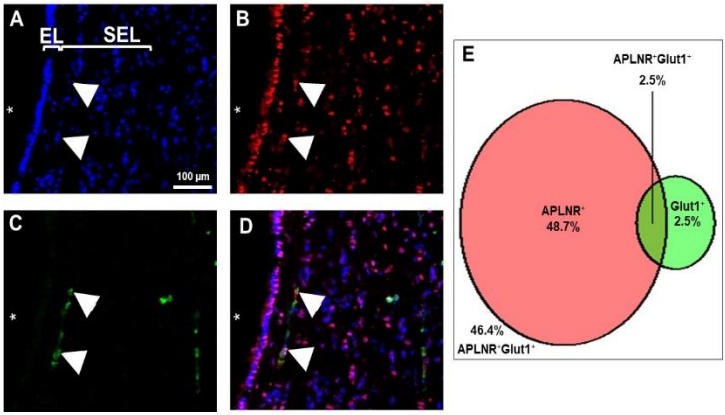

***Fig. 3.20**: (**A-D**) Immunohistochemical staining for APLNR (B) (red) and Glut1 (C) (green). All nuclei are stained with DAPI (A) (blue). An arrowhead indicates a double-positive cell for APLNR and Glut1 in the SEL. (D). Percentage ratio of individual cellular subpopulations: APLNR+, Glut1+, APLNR+/Glut1+ and APLNR-/Glut1- out of all cells (E).*

The apelinergic system consists of the apelin receptor and its ligand, apelin, which activates it. Based on this fact, we wanted to understand whether the signal for receptor activation, i.e., the apelin ligand, originates from the cerebrospinal fluid or if there are cells in the SVZ that secrete it. To achieve this, we conducted fluorescent immunohistochemical staining for APLN in combination with GFAP. We found individual cells (approximately 1 cell per coronal section, spanning the entire ventricle, located in the SVZ and positive for GFAP). Additionally, we observed extensive branching of cell processes, which either reached blood vessels or extended into one of the zones of the SVZ (***Fig. 3.21***).

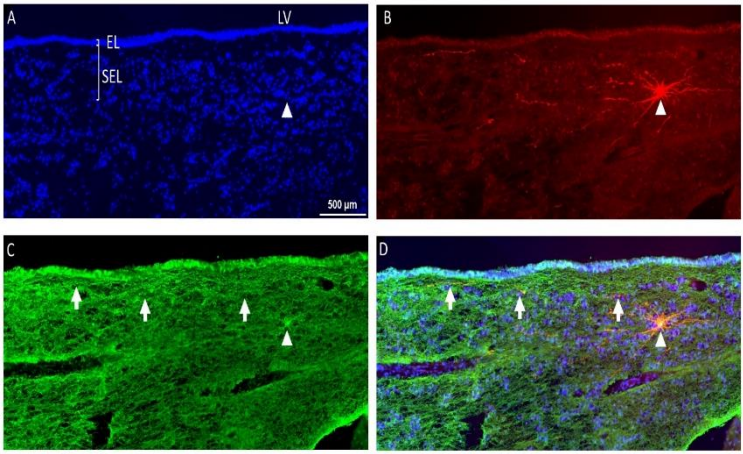

***Fig. 3.21**: (**A-D**) Immunohistochemical staining for APLN (B) (red) and GFAP (C) (green). All nuclei are stained with DAPI (A) (blue). An arrowhead indicates a double-positive cell for APLN and GFAP in the SEL, while arrows mark the cell processes extending to blood vessels and the ependyma (D).*

4. Discussion

4.1 Induction of gene expression following global ischemia

One of the obtained results showed an elevated expression of genes in the SVZ of an adult monkey following global ischemia. Our study focused on selecting genes expressed in different parts of the SVZ, associated either with the localization of stem cells in the stem cell niche, or with the signals they receive from it (see Chapter 6.1). The degree of expression was confirmed in two different ways, validating the accuracy of the results. Our observations demonstrate that cells containing mRNA for TNC, APLNR, GJA1, and CD38 are significantly upregulated in the subventricular layer. For all genes, we also observed enhanced expression in cells surrounding blood vessels. Various factors passing through either the blood vessels or the ependymal cells from the

cerebrospinal fluid may have a specific influence on the stem or progenitor cells in the SVZ.

4.2 Phenotypic expression of APLNR, TNC, CD38 and GJA1 in normal monkey

4.2.1 Phenotypic characterization of TNC in the normal monkey brain

The presented data up to this point necessitated a more detailed analysis of the cells expressing the mentioned genes. By combining GFAP, VIM, and BrdU markers, which label different groups of stem and progenitor cells, we were able to distinguish individual subpopulations based on the presence of the gene of interest in them.

Tenascin-C is an oligomeric extracellular protein containing monomers that in the central nervous system (CNS) is found around neurons and glia. It is also present in stem cell niches such as intestinal crypts, bone marrow, and hair follicles. Its presence has been described in various pathological conditions: tumor masses, inflammation, mechanical and chemical injuries, with its expression being heightened during tissue recovery[36,37]. As part of the extracellular matrix (ECM), Tenascin-C is directly associated with adhesion to other ECM proteins like fibronectin, integrin, collagen, periostin, fibrillin-2, and others[36,37]. Tenascin-C has the ability to activate the Epidermal Growth Factor Receptor (EGFR), thereby stimulating cellular proliferation. Tenascin-C can also be found in the SVZ in rodents, limited to the subependymal layer (SEL) and the rostral migratory stream (RMS). In the SVZ, it can be found in GFAP+ cells, most likely neuronal stem cells, but is absent in cells expressing markers such as PSA-NCAM (Polysialic Acid-Neural Cell Adhesion Molecule) marking neuroblasts, and Ascl1 (Achaete-scute homolog 1), marking transit-amplifying progenitor cells (TAPs) [38].

Summarizing the results of phenotyping, appropriate conclusions can be drawn about the nature of TNC+ cells in the SVZ of monkeys: they are expressed in a large portion of GFAP+ (qNSCs or aNSCs) cells (32%) and VIM+ (aNSCs or TAPs) cells (22%). The data from triple staining GFAP/TNC/BrdU can be interpreted as follows: the subpopulation GFAP+/TNC+/BrdU+ likely represents proliferating NSCs (aNSCs = 2%), while the subpopulation GFAP+/TNC+/BrdU- is most likely non-proliferative NSCs (qNSCs = 30%).

Due to the application of BrdU (5 days prior to euthanasia of the animals), it is expected to label not only aNSCs but also highly proliferative TAPs (see 5.10). Because it is present in both GFAP+ and VIM+ cells and the low expression of the gene in proliferative cells, we believe that TNC is likely expressed in a subpopulation of qNSCs. qNSCs may be primed for division, a state known as primed qNSCs, which is consistent with the ability of TNC to bind to EGFR and activate proliferation. It should be noted that there may be interspecies differences between mice and monkeys, potentially leading to disparities in the expression and ability of TNC to bind and activate EGFR.

Comparing the expression characteristics of TNC in monkeys and mice[38], we observe that TNC is expressed by neural stem cells, but unlike the phenotype in mice, in monkeys, TNC is also expressed by TAPs (TNC/Vim).

4.2.2 Phenotypic characterization of APLNR in the normal monkey brain

The APLNR is a G protein-coupled receptor of class A (rhodopsin-like receptor subclass A3), containing 380 amino acids, with the characteristic 7-transmembrane alpha-helical structure[39,40].

APLNR is widely distributed in the animal kingdom and is expressed in mouse, rat, human, monkey, and cattle. The ligands capable of activating the receptor are apelin-13, apelin-17, apelin-36, apelin-55, and Elabela/Toddler[41,42].

Both APLNR and APLN are found in both the central nervous system (CNS) and the peripheral nervous system (PNS) [5,43–45]. APLNR is detected in neurons, oligodendrocytes, and astrocytes, but not in microglia, while the ligand apelin is expressed by neurons but not astrocytes[46–50].

Based on the obtained phenotypic results, relevant conclusions can be drawn about the nature of APLNR+ cells in the SVZ of monkey brain. They are expressed in a large portion of GFAP+ (qNSCs or aNSCs) cells (74%) and VIM+ (aNSCs or TAPs) cells (40%). Only a small portion of them are proliferative (4%), with half (59%) of the proliferating cells expressing the gene. Since GFAP is expressed by neuronal stem cells, and Vim by neuronal stem cells and TAPs, triple staining for APLNR with these two markers indicates the presence of 9.9% triple-positive cells for APLNR+GFAP+VIM+, of which 15% are positive for APLNR, likely representing a subpopulation of aNSCs. Considering that GFAP marks qNSCs and aNSCs, and Vim marks aNSCs and TAPs, the Vim-negative subpopulation APLNR+GFAP+VIM- provides information about the presence of qNSCs in 50% of APLNR-expressing cells, while APLNR+GFAP-VIM+ gives information about the quantity of TAPs (8%).

The application of BrdU for only 5 days allows labeling of not only aNSCs but also highly proliferative TAPs (see 5.10). Data from double staining for APLNR/BrdU show that APLNR is expressed in a minimal extent by aNSCs and TAPs (4%). The indicated results can be interpreted as follows: the triple-positive APLNR+GFAP+VIM+ cells represent a subpopulation of aNSCs (15%), as GFAP is expressed in qNSCs and aNSCs, and Vim in aNSCs and TAPs. The APLNR+GFAP+VIM- subpopulation (50%) represents qNSCs due to the absence of Vim. This

demonstrates a decrease in APLNR expression in the transition from qNSCs to aNSCs to TAPs (qNSCs = APLNR+GFAP+VIM- (50%); aNSCs = APLNR+GFAP+VIM+ (15%); aNSCs/TAPs = APLNR/BrdU (4%); TAPs = APLNR+GFAP-VIM+ (8%).

Because APLNR is also expressed in blood vessels, we performed double and triple staining with markers VIM and GLUT1. From the obtained results, we found that 12% of all cells are double-positive for APLNR+GLUT1+, and 10.5% are triple-positive for APLNR+GLUT1+VIM+, confirming previous findings in rodents regarding the presence of APLNR in blood vessels.

4.2.3 Phenotypic characterization of GJA1 in the normal monkey brain

GJA1 (Connexin 43; Cx43) is a protein that plays a crucial role in intercellular communication. It is a transmembrane protein expressed in various tissues and organs, including the brain. GJA1 is expressed in both embryonic and adult subventricular zones, where it plays an important role in maintaining the proliferative abilities of neural stem cells (NSCs). Elevated expression of GJA1 is sufficient to stimulate the formation of functional extracellular channels, which is a critical condition for the maintenance and proliferation of NSCs. Additionally, GJA1 levels decrease when NSCs begin to differentiate into neurons[51,52].

Our results showed that GJA1 is expressed by both GFAP+ (aNSCs or qNSCs) cells (58%) and VIM+ (aNSCs or TAPs) cells (16.4%). The application method of BrdU would only label aNSCs or TAPs, with 4% of all BrdU+ cells being positive for GJA1. Our results also showed that less than 1% are proliferative aNSCs, as examined through triple staining for GFAP+GJA1+BrdU+. The subpopulation GFAP+GJA1+BrdU+ would label aNSCs (1.5% of GJA1), while GFAP+GJA1+BrdU- would

mark the subpopulation of qNSCs (57%). This demonstrates that GJA1 is highly expressed in qNSCs and to a lesser extent in aNSCs and TAPs.

These current results are consistent with recent data demonstrating the role of GJA1 in maintaining the proliferation and self-renewal of NSCs[53]. Through staining in combination with TNC, we additionally discovered a subpopulation of TNC-GJA1+ cells, which are negative for both VIM and BrdU. This demonstrates that these cells are qNSCs

4.2.4 Phenotypic characterization of CD38 in the normal monkey brain

CD38 is a 45 kDa transmembrane glycoprotein that possesses both receptor and enzyme-mediated functions. As a receptor, CD38 interacts with its ligand CD31, also known as PECAM-1[54]. The expression of CD31 is mainly observed in endothelial cells, where it is considered a constitutive marker. On the other hand, CD38 expression is observed in almost all areas of the brain and is found to be significantly higher in regions such as n. caudatus, palium, bulbus olfactorius, putamen, and thalamus. At the cellular level, CD38 is expressed in neurons, astrocytes, and microglial cells in both rodents and humans. In neurons, CD38 is primarily found in the perikaryon but is also present in dendrites. At the subcellular level in the mouse brain, CD38 is predominantly located on the plasma membrane but is also found intracellularly[51,55,56].

The phenotypic characterization of CD38 shows that the gene is expressed by GFAP+ cells (62.8%) and VIM+ cells (23.5%), with a small fraction of CD38+ cells proliferating (3.4%). Additional staining combining the markers GFAP+VIM+CD38+ revealed that a portion of the cells are triple-positive for GFAP+VIM+CD38+ (16%). Additionally, a distinct cellular fraction with the phenotype GFAP+VIM-CD38+ was observed (44%). These results indicate that the triple-positive GFAP+VIM+CD38+ cells represent aNSCs (16%), GFAP+VIM-CD38+

belong to qNSCs (46%), while GFAP-VIM+CD38+ cells are TAPs (7%). This demonstrates that the gene is expressed at high levels in qNSCs (46%), followed by a decrease in aNSCs (16%) and TAPs (7%). This illustrates a reduction in CD38 expression during the transition from qNSCs to aNSCs to TAPs (qNSCs = CD38+GFAP+VIM- (46%); aNSCs = APLNR+GFAP+VIM+ (16%); aNSCs/TAPs = APLNR/BrdU (3.4%); TAPs = APLNR+GFAP-VIM (7%)).

4.3 Phenotypic characterization of APLNR in the normal human brain

APLNR is also expressed in the human brain. Given that out of the four selected genes, APLNR represents the easiest one to pharmacologically influence through the ligand apelin, we used normal human brains to investigate its presence and phenotype in the SVZ. APLNR is found in all three layers of the SVZ (ependymal layer, gap zone, and subependymal layer). In combination with various markers for stem/progenitor cells, we discovered that APLNR is expressed by GFAP+ cells located in the astrocytic ribbon. Using a triple combination of APLNR/GFAP/Ki67, we determined that most of the APLNR+ cells are actively proliferating (16 out of 17 cells), with only 2 being triple-positive for GFAP/APLNR/Ki67. The presence of a few Ki67+ cells is in line with previous publications[57–60]. Proliferating ependymal cells were not detected, confirming that they are post-mitotic[61]. GFAPδ is an isoform of GFAP expressed only in a subpopulation of astrocytes in the subgranular zone of the hippocampus, subpallium, and in the astrocytic ribbon of the SVZ, with their processes located in the gap zone[62,63]. In addition, GFAPδ is expressed by proliferating cells, marked by PCNA and BrdU, present in neurospheres from the adult human brain, indicating that they represent slowly proliferating NSCs. Our results show that APLNR is also expressed in GFAPδ+ cells. We also observed that APLNR is expressed by other cell populations associated with various stages of neurogenesis (β-III-tubulin) or with cells associated with the stem cell niche (GLUT1, Iba1, s100b). 16% and 18% of APLNR+ cells have an unclear phenotype, likely representing TAPs. It

has been shown that the apelin ligand is expressed in the subventricular zone, with cells expressing the protein having numerous long processes, likely reaching cells expressing APLNR, thereby activating them. Additionally, the mechanism and significance of the apelinergic system in the neurogenic niche in humans need to be further elucidated.

4.5 Limitations of the current study

It is important to note some of the limitations of the current study. Firstly, the number of animals (Macaca fuscata = 3) and post-mortem brain tissues from humans (Homo sapiens = 3) used is insufficient for population-level analysis, only allowing for individual-level investigation. The same applies to the comparative analysis of rostro-caudal levels in Macaca fuscata, Mus musculus, and Callithrix jacchus, which was conducted using a public database where the brain of one animal is stained for only one gene, i.e., n = 1. However, this provides important direction for future studies related to the distribution of neural stem cells in non-human primate brains.

Regarding the presence of a rostro-caudal gradient of the proliferative marker Ki67, staining was performed only for Ki67, without double or triple staining with other markers. This provides information only about the absolute number of proliferating cells in different parts of the SVZ along the rostro-caudal axis, but not about their phenotypic characteristics.

Currently, in the field of research on neurogenesis in non-human primates, markers are used that can label more than one type of cellular subpopulation. For example, GFAP can label activated neural stem cells, inactive neural stem cells, as well as parenchymal astrocytes. This statement is true for other markers used in this dissertation such as Vim and BrdU. In our phenotypic characterization of adult macaques, a

marker for differentiating parenchymal astrocytes was not used when using antibodies for GFAP and Vim. Even the small possibility of the presence of parenchymal astrocytes in the SVZ in monkeys does not exclude the fact that they may be stained and represent a small part of the cells positive for these two markers. The same does not apply to the combinations Gene/GFAP/BrdU, as parenchymal astrocytes under normal conditions (i.e., without ischemia) do not divide. In the future, additional triple stainings GFAP/s100b/Gene and Vim/s100b/Gene would provide a better understanding of the expression of the genes studied by us in parenchymal astrocytes, as s100b specifically marks them. In addition, it would be beneficial to investigate the expression of the selected genes in combination with relatively specific markers expressed in neuroblasts and TAPs, such as DCX, β-III-tubulin, and EGFR, respectively.

Different levels of expression of GFAP and Vim were observed along the rostro-caudal axis. This means that the cellular subpopulations labeled by these two markers (aNSCs, qNSCs, TAPs) have different distributions along the rostro-caudal axis and possess different functions. It would be useful for future studies to conduct a more detailed characterization of the phenotype of the different genes selected by us along the rostro-caudal axis.

5 Conclusion

We present the first detailed study demonstrating increased expression of the genes TNC, APLNR, GJA1, CD38 following global ischemia in the largest neurogenic niche in non-human primates. Additionally, we show their rostro-caudal expression pattern in the ventricle of a normal monkey, which was quantitatively compared across different non-human primates. To understand the nature of cells expressing our selected genes, we conducted a phenotypic characterization using known stem cell markers. Our results indicate that in a normal monkey, these genes are likely expressed in neural stem cells at various stages of their differentiation. We also identified a combination

of markers specific to quiescent neural stem cells (TNC-GJA1+). Due to the potential pharmacological influence of APLNR, we conducted a detailed immunohistochemical characterization of cells expressing APLNR in the subventricular zone of adult humans without neurological or psychiatric disorders. Our results demonstrate that APLNR is expressed in all stages of neural stem cell differentiation, as well as in cells associated with the neurogenic niche. We also confirmed the presence of the apelin ligand in the SVZ of humans without pathology.

Future studies should elucidate the role and significance of TNC, CD38, and GJA1 in non-human primate neurogenesis. Clarifying the transcriptome at various rostro-caudal levels in primates would be of great importance. Finally, future research should investigate the molecular mechanisms underlying the role of APLNR in stem cell biology and explore the potential application of its ligands for therapies targeting central nervous system disorders characterized by neuronal death and increased neurogenesis and/or differentiation in the SVZ.

6 Conclusions

1. Global cerebral ischemia significantly increases the gene expression of APLNR, CD38, TNC, and GJA1 in the subventricular zone (SVZ) of adult macaques monkeys.
2. The expression of APLNR, CD38, TNC, and GJA1 along the rostro-caudal axis in the SVZ of adult macaques is heterogeneous..
3. Expression gradients of APLNR, CD38, TNC, and GJA1 along the rostro-caudal axis demonstrate interspecies differences.
4. In the SVZ of primates under normal conditions, the gene TNC marks a subpopulation of neural stem cells.
5. In a normal monkey, APLNR is likely expressed by "quiescent" neural stem cells, with expression decreasing during differentiation.
6. In a normal monkey, GJA1 is likely expressed by "quiescent" neural stem cells, with expression decreasing during differentiation.

7. The cellular subpopulation of TNC-GJA1+ represents a specific combination for identifying "quiescent" neural stem cells.

8. In a normal monkey, CD38 is likely expressed by "quiescent" neural stem cells, with expression decreasing during differentiation.

9. In humans, APLNR is expressed at various stages of differentiation of neural stem cells, as well as in cells associated with the neurogenic niche.

10. The apelin ligand is expressed by glial/neuronal cells in the SVZ of humans in the absence of pathology.

7 Contribution of the current dissertation work

1. For the first time, increased expression of the genes TNC, APLNR, GJA1, and CD38 is observed in a primate model of global cerebral ischemia.

2. The rostro-caudal expression of TNC, APLNR, GJA1, and CD38 is described for the first time in a normal monkey.

3. Differences in the rostro-caudal expression of TNC, APLNR, GJA1, and CD38 are demonstrated for the first time in three different non-human primates.

4. The detailed phenotypic characteristics of TNC, APLNR, GJA1, and CD38 in the SVZ of a normal monkey are documented for the first time.

5. The detailed phenotypic characteristics of APLNR in the SVZ of humans without pathology are clarified for the first time.

8 Publications related to the doctoral thesis

8.1 Stoyanov, D.S.; ***Ivanov, M.N.***; Yamashima, T.; Tonchev, A.B. Expression of Transcription Factor ZBTB20 in the Adult

Primate Neurogenic Niche under Physiological Conditions or after Ischemia. *Genes* **2022**, *13*, 1559. https://doi.org/10.3390/genes13091559

8.2 ***Ivanov, M.N.***; Pavlov, S.S.
Distribution and expression of Apelin/APJ system in the mammalian body- a review. BMR 2023, 32, xx-xx

9 Used Abbreviations

aa	Amino acids residues	MAX	MYC Associated Factor X
ADPRP	adenosine-5'-O-diphosphoribose	MCA	Middle cerebral artery
aNSC	activated NSC	MCM2	Minichromosome Maintenance Complex Component 2
AP	Alkalane phosphatese	mRNA	Messenger RNA
APLN	Apelin ligand	NAADP	Nicotinic acid adenine dinucleotide phosphate
APLNR	Apelin receptor	NADP	Nicotinamide adenine dinucleotide phosphate
Ascl1	Achaete-Scute Family BHLH Transcription Factor 1	NBT	Nitro Blue Tetrazolium
ATP	Adenosine triphosphate	NPC	Neural progenitor cell
BCIP	5-Bromo-4-chloro-3-indolyl phosphate	O.C.T.	Optimal cutting temperature compound
BrdU	Bromodeoxyuridine	OB	Olfactory bulb
CD38	Cluster of differentiation 38	Olig2	Oligodendrocyte transcription factor 2
cDNA	Comple	PBS	Phosphate-buffered saline
CNTF	Ciliary Neurotrophic Factor		
CXC24	Chemokines 24	PCNA	Proliferating cell nuclear antigen

DAPI	4′,6-diamidino-2-phenylindole	PECAM	Platelet endothelial cell adhesion molecule
DCX	Doublecortin	PK	Proteinase K Buffer
DEPC	Diethyl pyrocarbonate	Prom1	Prominin-1
DIG	Digoxigenin	PSA-NCAM	Polysialylated-neural cell adhesion molecule
EDTA	Ethylenediaminetetraacetic acid	PVSVZ zone	Perivascular subventricular
EdU	5-ethynyl-2′-deoxyuridine	qNSC	Quiescent Neuronal stem cell
EGFR	Epidermal growth factor receptor	RNA	Ribonucleic acid
EL	Ependymal layer	RNA-seq	RNA sequencing
FGF2	Fibroblast growth factor 2	Roi	Region of interest
FGFR1	fibroblast growth factor receptor 1	RT-PCR	Reverse transcription polymerase chain reaction
FICH	Fluorescent immunohistochemistry	SCD5	Stearoyl-CoA desaturase 5
FISH	Fluorescent in situ hybridisation	SDF1	Stromal cell-derived factor 1
GFAP	Glial fibrillary acidic protein	SEL	Subependymal layer
GJA1	Gap Junction Protein Alpha 1	SGZ	Subgranular zone
GLAST	Glutamate aspartate Transporter	STR	Striatum
Glut1	Glucose transporter 1	SVZ	Subventricular zone
i.m.	intramuscular injection	TAPs	Transient Amplification Progenitors
i.v.	Intravenous	TNC	Tenascin c
Iba1	Ionized calcium-binding adapter molecule 1	tRNA	Transport ribonucleic acid
IHC	Immunohistochemistry	TUC4	Turned On After Division
ISH	In situ hibridisation	Tuj1	III beta-tubulin
kDA	Kilodalton	VEGF	Vascular Endothelial Growth Factor
Ki67	Marker of proliferation Kiel 67	WB	Western Blot
Kif2A	Kinesin Family Member 2A	Wnt	Wingless
LGR5	Leucine-rich repeat-containing G-protein coupled receptor 5	ZBTB20	Zinc Finger And BTB Domain Containing 20

10 Acknowledgments

- • Thank you to my advisor, **Assoc. Prof. Pavlov**, for the support and guidance, for answering my endless questions.
- Thank you to **Prof. Tonchev** for the help, trust, and support! Thank you for your endless patience.
- • To Dimo, Lora, and Andon for the hours of discussion, debating, and the friendly atmosphere
- Thank you to the lab assistants **Velina Kenovska, Elena Boeva**, **Neranza Koleva**, and **Gabriela Dimitrova** for their responsibility and precision in preparing the histological samples.
- Thank you to the preparators **Lilya Daskalova** and **Dyliana Dimitrova** for their help in conducting the practical exercises.
- Thank you to my colleagues from the Department of Anatomy and Cell Biology for the wonderful working environment and moral support.
- Thank you to my colleagues from the Department of Anatomy and Cell Biology for the wonderful working environment and moral support.
- Above all, to my big family for the help, support, and belief in me. I want to thank them for being there for me even when I was absent in body or spirit.

1. Codega, P. *et al.* Prospective Identification and Purification of Quiescent Adult Neural Stem Cells from Their In Vivo Niche. *Neuron* **82**, 545–559 (2014).
2. Kam, M. *et al.* The cellular composition and morphological organization of the rostral migratory stream in the adult human brain. *J. Chem. Neuroanat.* **37**, 196–205 (2009).
3. Brossa, A. *et al.* Role of CD133 Molecule in Wnt Response and Renal Repair. *Stem Cells Transl. Med.* **7**, 283–294 (2018).
4. Hara, K. *et al.* Anomaly in aortic arch alters pathological outcome of transient global ischemia in Rhesus macaques. *Brain Res.* **1286**, 185–191 (2009).
5. Chongtham, M. C. *et al.* Transcriptome Response and Spatial Pattern of Gene Expression in the Primate Subventricular Zone Neurogenic Niche After Cerebral Ischemia. *Front. Cell Dev. Biol.* **8**, 1–17 (2020).
6. Lein, E. S. *et al.* Genome-wide atlas of gene expression in the adult mouse brain. *Nature* **445**, 168–176 (2007).

7. Yaylaoglu, M. B. *et al.* Comprehensive expression atlas of fibroblast growth factors and their receptors generated by a novel robotic in situ hybridization platform. *Dev. Dyn.* **234**, 371–386 (2005).
8. *In Situ Hybridization Methods*. vol. 99 (Springer New York, 2015).
9. Kõressaar, T. *et al.* Primer3-masker: Integrating masking of template sequence with primer design software. *Bioinformatics* **34**, 1937–1938 (2018).
10. Saleem, K. S. K. & Logothetis, N. K. N. *A combined MRI and Histology Atlas of the rhesus monkey brain in stereotazic coordinates*. *Academic Press, London* (Elsevier, 2007).
11. CARSON, J. P., EICHELE, G. & CHIU, W. A method for automated detection of gene expression required for the establishment of a digital transcriptome-wide gene expression atlas. *J. Microsc.* **217**, 275–281 (2005).
12. Speel, E. J. M., Hopman, A. H. N. & Komminoth, P. Amplification Methods to Increase the Sensitivity of In Situ Hybridization: Play CARD(S). *J. Histochem. Cytochem.* **47**, 281–288 (1999).
13. Chao, J., DeBiasio, R., Zhu, Z., Giuliano, K. A. & Schmidt, B. F. Immunofluorescence signal amplification by the enzyme-catalyzed

deposition of a fluorescent reporter substrate (CARD). *Cytometry* **23**, 48–53 (1996).

14. Tonchev, A. B., Yamashima, T., Sawamoto, K. & Okano, H. Enhanced proliferation of progenitor cells in the subventricular zone and limited neuronal production in the striatum and neocortex of adult macaque monkeys after global cerebral ischemia. *J. Neurosci. Res.* **81**, 776–788 (2005).
15. Tonchev, A. B., Yamashima, T., Zhao, L., Okano, H. J. & Okano, H. Proliferation of neural and neuronal progenitors after global brain ischemia in young adult macaque monkeys. *Mol. Cell. Neurosci.* **23**, 292–301 (2003).
16. Bourne, R. & Bourne, R. ImageJ. *Fundam. Digit. Imaging Med.* **9**, 185–188 (2010).
17. Schindelin, J. *et al.* Fiji: an open-source platform for biological-image analysis. *Nat. Methods* **9**, 676–682 (2012).
18. Carpenter, A. E. *et al.* CellProfiler: Image analysis software for identifying and quantifying cell phenotypes. *Genome Biol.* **7**, (2006).

19. Lamprecht, M. R., Sabatini, D. M. & Carpenter, A. E. CellProfiler™: Free, versatile software for automated biological image analysis. *BioTechniques* **42**, 71–75 (2007).

20. Shihavuddin, A. *et al.* Smooth 2D manifold extraction from 3D image stack. *Nat. Commun.* **8**, 1–8 (2017).

21. Darbon, J., Cunha, A., Chan, T. F., Osher, S. & Jensen, G. J. Fast nonlocal filtering applied to electron cryomicroscopy. *2008 5th IEEE Int. Symp. Biomed. Imaging Nano Macro Proc. ISBI* 1331–1334 (2008) doi:10.1109/ISBI.2008.4541250.

22. Buades, A., Coll, B. & Morel, J.-M. Non-Local Means Denoising. *Image Process. Line* **1**, 208–212 (2011).

23. Legland, D., Arganda-Carreras, I. & Andrey, P. MorphoLibJ: Integrated library and plugins for mathematical morphology with ImageJ. *Bioinformatics* **32**, 3532–3534 (2016).

24. Soille, P. *Morphological Image Analysis*. (Springer Berlin Heidelberg, 1999). doi:10.1007/978-3-662-03939-7.

25. Agresti, A. *Analysis of Ordinal Categorical Data*. (John Wiley & Sons, Inc., 2010). doi:10.1002/9780470594001.

26. Kushary, D., Davison, A. C. & Hinkley, D. V. Bootstrap Methods and Their Application. *Technometrics* **42**, 216 (2000).
27. Carpenter, J. & Bithell, J. Bootstrap confidence intervals: when, which, what? A practical guide for medical statisticians. *Stat. Med.* **19**, 1141–1164 (2000).
28. R Core Team. R: A Language and Environment for Statistical Computing. Preprint at (2020).
29. Team, Rs. RStudio: Integrated Development Environment for R. (2020).
30. Wickham, H. *et al.* Welcome to the Tidyverse. *J. Open Source Softw.* **4**, 1686 (2019).
31. Robin, X. *et al.* pROC: an open-source package for R and S+ to analyze and compare ROC curves. *BMC Bioinformatics* **12**, 77 (2011).
32. Ming, G. li & Song, H. Adult Neurogenesis in the Mammalian Brain: Significant Answers and Significant Questions. *Neuron* **70**, 687–702 (2011).

33. Chaker, Z., Codega, P. & Doetsch, F. A mosaic world: puzzles revealed by adult neural stem cell heterogeneity. *Wiley Interdiscip. Rev. Dev. Biol.* **5**, 640–658 (2016).

34. Young, C. C. *et al.* Ependymal ciliary dysfunction and reactive astrocytosis in a reorganized subventricular zone after stroke. *Cereb. Cortex* **23**, 647–659 (2013).

35. Ayanlaja, A. A. *et al.* Distinct features of doublecortin as a marker of neuronal migration and its implications in cancer cell mobility. *Front. Mol. Neurosci.* **10**, 1–13 (2017).

36. Midwood, K. S., Chiquet, M., Tucker, R. P. & Orend, G. Tenascin-C at a glance. *J. Cell Sci.* **129**, 4321–4327 (2016).

37. Tucić, M., Stamenković, V. & Andjus, P. The Extracellular Matrix Glycoprotein Tenascin C and Adult Neurogenesis. *Front. Cell Dev. Biol.* **9**, 1–12 (2021).

38. Kazanis, I., Belhadi, A., Faissner, A. & Ffrench-Constant, C. The Adult Mouse Subependymal Zone Regenerates Efficiently in the Absence of Tenascin-C. *J. Neurosci.* **27**, 13991–13996 (2007).

39. Ma, Y. *et al.* Structural Basis for Apelin Control of the Human Apelin Receptor. *Structure* **25**, 858-866.e4 (2017).

40. Pitkin, S. L., Maguire, J. J., Bonner, T. I. & Davenport, A. P. International Union of Basic and Clinical Pharmacology . LXXIV . Apelin Receptor Nomenclature , Distribution , Pharmacology , and Function. **62**, 331–342 (2010).
41. Chng, S. C., Ho, L., Tian, J. & Reversade, B. ELABELA: A hormone essential for heart development signals via the apelin receptor. *Dev. Cell* **27**, 672–680 (2013).
42. Pauli, A. *et al.* Toddler: An embryonic signal that promotes cell movement via apelin receptors. *Science* **343**, (2014).
43. De Mota, N. *et al.* Apelin, a potent diuretic neuropeptide counteracting vasopressin actions through inhibition of vasopressin neuron activity and vasopressin release. *Proc. Natl. Acad. Sci.* **101**, 10464–10469 (2004).
44. Reaux, A., Gallatz, K., Palkovits, M. & Llorens-Cortes, C. Distribution of apelin-synthesizing neurons in the adult rat brain. *Neuroscience* **113**, 653–662 (2002).
45. Reaux, A. *et al.* Physiological role of a novel neuropeptide, apelin, and its receptor in the rat brain. *J. Neurochem.* **77**, 1085–1096 (2001).

46. Choe, W. *et al.* Functional expression of the seven-transmembrane HIV-1 co-receptor APJ in neural cells. *J. Neurovirol.* **6**, (2000).
47. Puffer, B. A. *et al.* Expression and coreceptor function of APJ for primate immunodeficiency viruses. *Virology* **276**, 435–444 (2000).
48. Medhurst, A. D. *et al.* Pharmacological and immunohistochemical characterization of the APJ receptor and its endogenous ligand apelin. *J. Neurochem.* **84**, 1162–1172 (2003).
49. O'Donnell, L. A. *et al.* Apelin, an endogenous neuronal peptide, protects hippocampal neurons against excitotoxic injury. *J. Neurochem.* **102**, 1905–1917 (2007).
50. Zeng, X. J., Yu, S. P., Zhang, L. & Wei, L. Neuroprotective effect of the endogenous neural peptide apelin in cultured mouse cortical neurons. *Exp. Cell Res.* **316**, 1773–1783 (2010).
51. Cheng, A. *et al.* Gap junctional communication is required to maintain mouse cortical neural progenitor cells in a proliferative state. *Dev. Biol.* **272**, 203–216 (2004).
52. Cx43 in neural progenitors.

53. Genet, N. *et al.* Connexin 43-mediated neurovascular interactions regulate neurogenesis in the adult brain subventricular zone. *Cell Rep.* **42**, 112371 (2023).

54. Malavasi, F. *et al.* Evolution and Function of the ADP Ribosyl Cyclase/CD38 Gene Family in Physiology and Pathology. *Physiol. Rev.* **88**, 841–886 (2008).

55. Guerreiro, S., Privat, A.-L., Bressac, L. & Toulorge, D. CD38 in Neurodegeneration and Neuroinflammation. *Cells* **9**, 471 (2020).

56. Braidy, N. *et al.* Mapping NAD+ metabolism in the brain of ageing Wistar rats: potential targets for influencing brain senescence. *Biogerontology* **15**, 177–198 (2014).

57. Kukekov, V. G. *et al.* Multipotent Stem/Progenitor Cells with Similar Properties Arise from Two Neurogenic Regions of Adult Human Brain. *Exp. Neurol.* **156**, 333–344 (1999).

58. Quiñones-Hinojosa, A. *et al.* Cellular composition and cytoarchitecture of the adult human subventricular zone: A niche of neural stem cells. *J. Comp. Neurol.* **494**, 415–434 (2006).

59. Wang, C. *et al.* Identification and characterization of neuroblasts in the subventricular zone and rostral migratory stream of the adult human brain. *Cell Res.* **21**, 1534–1550 (2011).

60. Dennis, C. V., Suh, L. S., Rodriguez, M. L., Kril, J. J. & Sutherland, G. T. Human adult neurogenesis across the ages: An immunohistochemical study. *Neuropathol. Appl. Neurobiol.* **42**, 621–638 (2016).

61. Spassky, N. Adult Ependymal Cells Are Postmitotic and Are Derived from Radial Glial Cells during Embryogenesis. *J. Neurosci.* **25**, 10–18 (2005).

62. Roelofs, R. F. *et al.* Adult human subventricular, subgranular, and subpial zones contain astrocytes with a specialized intermediate filament cytoskeleton. *Glia* **52**, 289–300 (2005).

63. van den Berge, S. A. *et al.* Longterm quiescent cells in the aged human subventricular neurogenic system specifically express GFAP-δ. *Aging Cell* **9**, 313–326 (2010).